What Makes a Good Solar Cell?

Thomas Kirchartz* and Uwe Rau

Recent years have seen a substantial efficiency improvement for a variety of solar cell technologies as well as the rise of a new class of photovoltaic absorber materials, the metal-halide perovskites. Conversion efficiencies that are coming closer and closer to the thermodynamic limits require a physical description of the corresponding solar cells that is compatible with those limits. This progress report summarizes recent work on the interdependence of basic material properties of semiconductor materials with their efficiency potential as photovoltaic absorbers. The connection of the classical Shockley–Queisser approach, with the band gap energy as the only parameter, to a more general radiative limit and to situations where nonradiative recombination dominates is discussed. The authors delineate a consistent loss analysis that enables a quantitative comparison between different solar cell technologies. In a next step, bulk material properties that influence the photovoltaic performance of a semiconductor like absorption coefficient, densities of states of the free carriers, or phonon energies are considered. It is shown that variations of these properties have a big influence on the optimized design of a solar cell but not necessarily on the achievable efficiency.

1. Introduction

In recent years, two main developments have shaped the research field of photovoltaics: first, the cost reduction in crystalline Si photovoltaics[1] implies that in order to reduce system cost, the area-related balance of system costs becomes increasingly important.[2] In consequence research has to focus definitely on high-efficiency concepts as opposed to low-cost–low-efficiency approaches. The second development was the discovery[3–6] of metal-halide perovskites as a novel material class for photovoltaic absorber materials. The development of the laboratory-scale efficiencies of metal-halide perovskites represents an unprecedented success story that has led to an efficiency increase from ≈10% to 22.7%[7] within 5 years. While this rapid rise was certainly based on the community having accumulated substantial knowledge on how to design good

solar cells, the speed is partly also due to quite peculiar properties of these metal-halide perovskites.

In particular, the second development triggered renewed interest in finding further promising photovoltaic materials based on computational or experimental material screening.[8–19] Such screening efforts would initially require a profound understanding of the key ingredients that are crucial for photovoltaic performance on a microscopic level.[20,21] This question of how to identify future promising materials for photovoltaics is closely connected to the question of how to explain the surprisingly high performance of some quite specific families of semiconductors. A typical example for a highly complex material used successfully in photovoltaics is $Cu(In,Ga)Se_2$, which has achieved photovoltaic power conversion efficiencies approaching 23%[22,23] being a polycrystalline semiconductor while all equally well or better performing materials were monocrystalline (Si or III/V materials).[24] Admittedly, the development of $Cu(In,Ga)Se_2$ took decades starting in the early 1970s[25,26] until the community had discovered and developed all the necessary techniques and skills[22,23,27–33] that were necessary to achieve efficiencies of >22%. Thus, it was quite surprising for the photovoltaic community that lead-halide perovskites managed the same efficiency achievement within only a few years.[34–37] While lead-halide perovskites certainly have exceptional electronic and optical properties[38–40] for a solution processed material, issues with stability[41,42] and toxicity[43–45] imply that the community is constantly looking for new variations of this material, e.g., lead-free perovskites[46–55] or lead-based perovskites with two, three, or even four cations[56–58] on the same lattice position. In addition, materials consisting of completely different elements and/or materials growing in different crystal structures are screened or closely analyzed for their applicability in photovoltaics and optoelectronics in general, using both computational and experimental methods.[59]

All these developments require a clearer picture of which parameters are crucial or at least helpful for enabling good solar cells. The purpose of this progress report is to establish the key criteria that make up a good solar cell material and discuss them on various levels of abstraction. These are shown in **Figure 1** and range from thermodynamic efficiency limits describing the solar cell using external parameters like quantum efficiencies via the description of the device via internal parameters (e.g., lifetimes, mobilities, and absorption coefficients) to the microscopic level of band structures and

Prof. T. Kirchartz, Prof. U. Rau
IEK5-Photovoltaics
Forschungszentrum Jülich
52425 Jülich, Germany
E-mail: t.kirchartz@fz-juelich.de

Prof. T. Kirchartz
Faculty of Engineering and CENIDE
University of Duisburg-Essen
Carl-Benz-Str. 199, 47057 Duisburg, Germany

The ORCID identification number(s) for the author(s) of this article can be found under https://doi.org/10.1002/aenm.201703385.

**ADVANCED
SCIENCE NEWS**

www.advancedsciencenews.com

**ADVANCED
ENERGY
MATERIALS**

www.advenergymat.de

phonon energies. A starting point for this discussion is the Shockley–Queisser (SQ) theory,[60] which gives a first indication of what is necessary: a certain band gap depending on whether it is a single junction, tandem, or even triple cell, we are aiming at. The Shockley–Queisser theory is certainly the highest useful level of abstraction which, consequently, contains only minimum information on how the solar cell absorber material should look like. From this limiting situation, we decrease the level of abstraction and first look at the optical properties of the material such as the complex refractive index. Nearly complete absorption of photons, however, is easily achieved in extremely thick semiconductor layers. Thus, the next stage does require taking the effect of nonradiative recombination and subsequently finite mobilities on the thickness dependence of photovoltaic efficiencies into account. This brings us to the point, where we will understand that absorption coefficient α, charge carrier mobility μ, and charge carrier lifetime τ are the three key parameters that determine efficiency on a device level. However, they do not yet answer how α, μ, and τ depend on microscopic material parameters.

The final section of our review, therefore, brings us to the question of how the microscopic structure of the photovoltaic absorber material affects photovoltaic performance via its influence on parameters such as phonon energies, trap densities, or how the strength of electron–phonon coupling described by the Huang–Rhys factor should affect α, μ, and τ and subsequently photovoltaic performance. On every level of abstraction, we will discuss how to calculate or simulate photovoltaic efficiency based on the macroscopic or microscopic input parameters discussed in each section.

2. Shockley–Queisser Limit

The SQ model[60] is a widely used approach to calculate the efficiency limit of a single junction solar cell based on the principle of detailed balance between absorption and emission of light. In addition to its direct results, the SQ approach provides the possibility of extending and adapting the detailed balance theory to a range of scenarios not discussed in the original paper. These scenarios include multijunction solar cells,[61,62] fluorescent converters,[63,64] organic solar cells,[65,66] or various types of hot carrier and multiple exciton generation solar cells.[67–69]

The SQ model treats the solar cell as a black box with a step-function-like absorptance being 1 above the band gap E_g and 0 below. In addition, every photon creates only one electron–hole pair, and charge carriers of both polarities will then be able to reach their respective contacts. Thus, the short-circuit current density of the solar cell in the SQ limit follows directly from

$$J_{sc,SQ} = q \int_{E_g}^{\infty} \phi_{sun}(E)\, dE \tag{1}$$

where q is the elementary charge and ϕ_{sun} is the solar spectrum in units of cm^{-2} s^{-1} eV^{-1}. Equation (1) already includes the first major loss mechanism of solar cells in the SQ limit, namely the loss of low-energy photons with energies below the band gap E_g which are not absorbed by the solar cell.

Thomas Kirchartz is currently a Professor of Electrical Engineering and Information Technology at the University Duisburg-Essen and the Head of the Department of analytics and simulation and the group of organic and hybrid solar cells at the Research Centre Jülich (Institute for Energy and Climate Research). Previously he was a Junior Research Fellow at Imperial College London. His research interests include the fundamental understanding of photovoltaic devices as well as their characterization and simulation.

Uwe Rau is currently the Director of the Institute for Energy and Climate Research-5 (Photovoltaics) at Research Centre Jülich. He is also Professor at RWTH Aachen, Faculty of Electrical Engineering and Information Technology where he holds the Chair of Photovoltaics. Previously, he was a senior researcher at the University Stuttgart as well as a postdoc at the University Bayreuth and at the Max-Planck-Institute for Solid State Research in Stuttgart. His research interest covers electronic and optical properties of semiconductors and semiconductor devices, especially characterization, simulation, and technology of solar cells and solar modules.

The principle of detailed balance[70] requires that absorption is only possible when emission of photons is also allowed. This statement is equivalent to the saying that Kirchhoff's law[71] equating the absorptance and emissivity of a black body holds not only for thermal radiation but also for luminescence. Thus, we can calculate the excess luminescence flux $\Delta\Phi_{lum}$ emitted from the solar cell via[72]

$$\Delta\Phi_{lum} = \int_{E_g}^{\infty} \phi_{bb}(E)\, dE \left[\exp\left(\frac{qV}{kT}\right) - 1 \right] \tag{2}$$

with $V = \Delta E_f/q$ being the internal voltage that is equal to the quasi-Fermi level splitting ΔE_f divided by the elementary charge q within the device. Here

$$\phi_{bb}(E) = \frac{2\pi E^2}{h^3 c^2} \frac{1}{\left[\exp\left(E/kT\right) - 1\right]} \approx \frac{2\pi E^2}{h^3 c^2} \exp\left(\frac{-E}{kT}\right) \tag{3}$$

is the black body spectrum at temperature T of the solar cell, h is the Planck's constant, and c is the speed of light.

**ADVANCED
SCIENCE NEWS**
www.advancedsciencenews.com
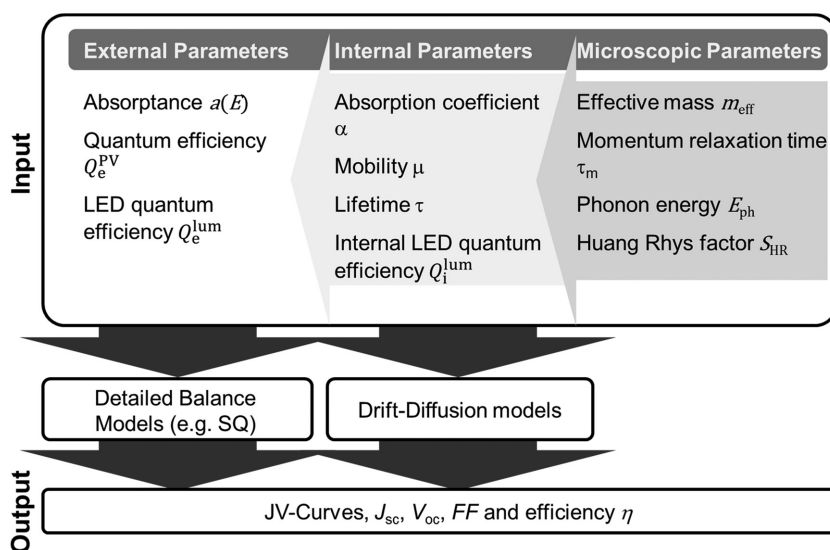
**ADVANCED
ENERGY
MATERIALS**
www.advenergymat.de

Figure 1. Outline of the paper illustrating the different models of a solar cell, which use a different level of abstraction. The first situation involves looking at the solar cell from the outside, and describing it essentially using the photovoltaic and the light-emitting diode (LED) or luminescence quantum efficiencies. Models based on detailed balance such as the SQ model and variations thereof may be used to calculate the current voltage curve. If we start with internal parameters such as absorption coefficient, mobility, or lifetime, we typically use drift–diffusion models to calculate the J–V curve and subsequently the efficiency. The last step is trying to understand the internal parameters from the microscopic properties of the material such as the effective mass, the momentum relaxation time, the phonon energy, or the Huang–Rhys factor which describes the strength of electron–phonon coupling.

square brackets can be interpreted as the saturation current density

$$J_{0,SQ} = q \int_{E_g}^{\infty} \phi_{bb}(E, T = 300 \text{ K}) \, dE \tag{4}$$

in the SQ limit. Thus, the current–voltage curve under illumination in the SQ limit follows as

$$J = J_{0,SQ} \left[\exp\left(\frac{qV}{kT}\right) - 1 \right] - J_{sc,SQ} \tag{5}$$

and the open-circuit voltage $V_{oc,SQ}$ is

$$V_{oc,SQ} = \frac{kT}{q} \ln\left(\frac{J_{sc,SQ}}{J_{0,SQ}} + 1\right) \tag{6}$$

In order to calculate the efficiency, we divide the maximum of the extracted power density $P = -JV$ by the incoming power density, that is

$$\eta = \frac{\max(P)}{\int_0^{\infty} E\phi_{sun}(E) \, dE} \tag{7}$$

Equations (2) and (3) imply that the carriers in the bands are already thermalized before they emit luminescence thus causing a second major loss mechanism of the SQ limit, namely, the energy loss due to thermalization of electron–hole pairs with energy much greater than the band gap E_g. In the SQ limit, radiative recombination is the only allowed recombination process. In an ideal solar cell, there is no dark current possible without recombination, i.e., the dark current is the recombination current in the dark. Thus, the dark current density J_d–voltage V curve of the ideal solar cell is given by $J_d = q\Delta\Phi_{lum}(V)$. Equation (2) has the mathematical form of a diode current–voltage curve, and therefore the prefactor before the

Figure 2a shows the efficiency for a single junction solar cell based on the methodology derived above. The maximum efficiency in the SQ limit for a single junction solar cell without optical concentration and assuming the AM1.5G spectrum as defined in ref. [73] is about 33%. This maximum efficiency is reached or nearly reached for a range of band gaps around 1.1–1.45 eV which includes most technologically important semiconductors such as crystalline Si, GaAs, and Cu(In,Ga)Se$_2$ over a wide range of In to Ga ratios as well as CdTe.

The SQ model allows us to calculate the limiting efficiency of a solar cell without considering its internal properties. We do not have to specify the cell thickness, the absorption
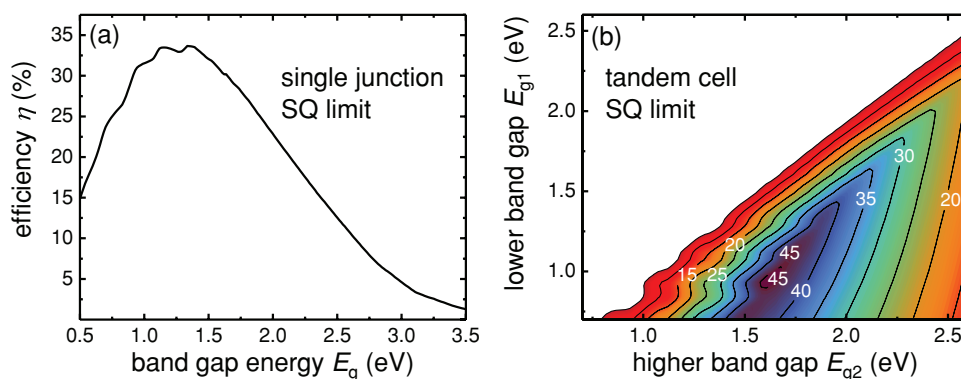

Figure 2. Efficiency in the SQ limit for a) a single junction solar cell and b) a tandem solar cell. For the calculations we assumed $T = 300$ K and illumination via the AM1.5G spectrum tabulated in ref. [73] (without concentration). For the case of the tandem solar cell, we neglected optical coupling between the two subcells.

ADVANCED
SCIENCE NEWS
www.advancedsciencenews.com

ADVANCED
ENERGY
MATERIALS
www.advenergymat.de

coefficient of the absorber material, or the charge-carrier mobility. In addition, we know that we cannot overcome the SQ limit without circumventing one of the assumptions used to derive the limit. However, a major merit of the SQ paper is the clarity of the restricting assumptions that give immediate hints toward the directions to overcome the limit. One of these directions is the use of more than one semiconductor material. The use of multijunction solar cells, with absorbers of various band gaps, reduces the thermalization losses, i.e., the energy loss that follows when photons with energy larger than E_g are absorbed and the photogenerated carriers relax toward the band edges. Likewise, the losses due to nonabsorption of low-energy photons are also reduced by the proper choice of lower band gap energies within the multijunction stack. Figure 2b shows the efficiencies of tandem solar cells in the SQ limit, which reach 45% even without concentration. Achieving these efficiencies requires in addition to low band gap solar cells in the lower range of the ones ideal for single junction solar cells ($\approx$1.1 eV) also solar cells with higher band gaps of >1.45 eV which was the upper end of the range of ideal single junction solar cell band gaps. While ideal tandem efficiencies can be reached with combinations such as $E_{g1} \approx 0.9$ eV and $E_{g2} \approx 1.6$ eV, the technologically most relevant combinations might be, in the future, those which combine the band gaps of Si or Cu(In,Ga)Se$_2$ of around $E_{g1} \approx 1.1$ eV with band gaps in the range of $E_{g2} \approx 1.75$ eV which would then be the ideal high band gap partner material.

3. Describing Solar Cells with External Parameters

The assumption of a step function for the absorptance of the solar cell is the key simplification of the SQ approach reducing the number of physical parameters for the description of the problem to one, namely the band gap energy. It is straight forward to extend the SQ approach to the more general situation of an arbitrary absorptance that can be determined experimentally or theoretically for a specific photovoltaic absorber. Thus, it is possible to determine an efficiency limit similar to the SQ approach that is specific to a particular sample or device. We will call this limit the "radiative" limit to distinguish it from the original SQ limit. This radiative limit is not unique for a certain material because the absorptance depends on the thickness of the layers and on the optical properties of interfaces (i.e., scattering and reflection, etc.). We will discuss the issue of optical models in Section 4 whereas for the moment we will limit ourselves to external, measureable parameters such as the absorptance (E) and photovoltaic quantum efficiency Q_e^{PV}.

If we assume that the quasi-Fermi level splitting ΔE_f is constant over the thickness of the device, i.e., the mobility is infinitely (or sufficiently) high, the luminescence flux is[72]

$$\phi_{em}(E) = a(E)\phi_{bb}(E)\left\{\exp\left(\frac{\Delta E_f}{kT}\right)-1\right\} \tag{8}$$

If the quasi-Fermi level splitting changes within the solar cell absorber volume, the calculation of the luminescence emission becomes more complex.[74] However, an important

generalization of the SQ approach is given by the optoelectronic reciprocity relation. Under the assumptions of Rau,[75] the electroluminescence emission is given by

$$\phi_{em}(E) = Q_e^{PV}(E)\phi_{bb}(E)\left\{\exp\left(\frac{qV}{kT}\right)-1\right\} \tag{9}$$

where V is the internal voltage defined as the quasi-Fermi level splitting at the edge of the space-charge region and the neutral base of a p–n-junction-type solar cell. The assumptions required for the validity of Equation (9) are that charge transport is by diffusion rather than by drift and that recombination is linear in minority carrier concentration.[75] These conditions are typically valid in the base of a p–n-junction at typical light intensities and voltages relevant for photovoltaic operation. The conditions are not valid in fully depleted thin-film solar cells.[74] Note that with $Q_e^{PV}(E) = a(E)$, Equation (8) follows from Equation (9), and with $a(E)$ equaling a step function, we recover Equation (2), i.e., the original SQ approach. Furthermore, Equation (9) together with the superposition of electro- and photoluminescence[76] provides the base for the quantitative (electro- and photo-) luminescence analysis of solar cells (see, e.g., ref. [77]).

In the following, we will discuss the radiative limit using the external quantum efficiency Q_e^{PV} keeping in mind that the external quantum efficiency can be replaced by the absorptance of the photovoltaic absorber layer if the mobilities are sufficiently high.[74] We now replace the step function in Equations (1) and (4) by Q_e^{PV} and obtain the short-circuit current density

$$J_{sc} = q\int_0^\infty Q_e^{PV}(E)\phi_{sun}(E)\,dE \tag{10}$$

and the radiative saturation current density

$$J_0^{rad} = q\int_0^\infty Q_e^{PV}(E)\phi_{bb}(E)\,dE \tag{11}$$

Comparing the SQ limit with a step-function-like absorptance and the radiative limit allows us to quantify losses due to the quantum efficiency not increasing abruptly above the band gap. This lack of abruptness may be due to disordered absorption edges, low absorption coefficients as observed, e.g., in indirect semiconductors or the lack of efficient light-trapping schemes. **Figure 3** illustrates the concepts of the Shockley–Queisser limit as discussed in Section 2 with the radiative limit discussed in the present Section 3. Figure 3 compares the power density per energy interval of the AM1.5G spectrum with the power density of a solar cell in the SQ limit and the power density for a real cell. Figure 3a shows the SQ limit for $E_g = 1.12$ eV and experimental data of a crystalline Si solar cell[78] while Figure 3b shows the SQ limit for $E_g = 1.6$ eV and a lead-halide perovskite solar cell.[79] The area under the curves is in all cases proportional to the power at the maximum power point and therefore also the efficiency. The power losses for the SQ limit are caused by thermalization, radiative recombination, and transmission of photons below the band gap. The additional losses for the Si and perovskite solar cells are due to a slight reduction of the photovoltaic quantum efficiency relative to the step function
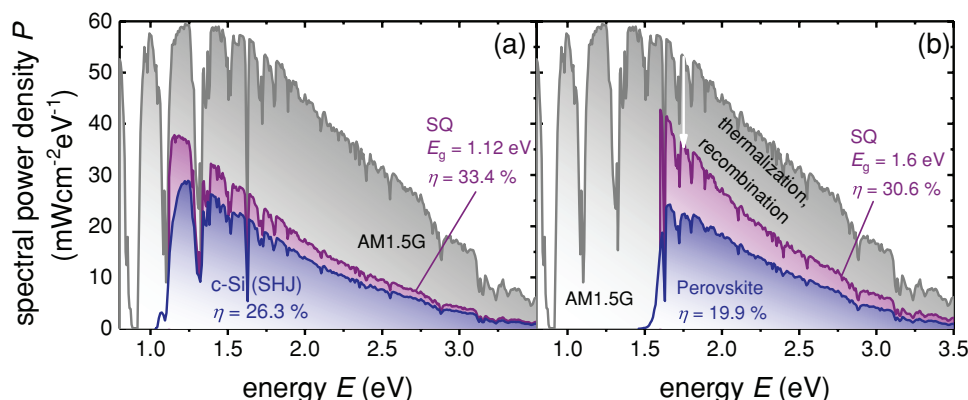
ADVANCED
SCIENCE NEWS

www.advancedsciencenews.com

ADVANCED
ENERGY
MATERIALS

www.advenergymat.de

Figure 3. Power density per energy interval for the AM1.5G spectrum as well as for two real solar cells: a) crystalline Si, data (EQE, V_{oc}, FF) taken from ref. [78] and b) lead-halide perovskite, data taken from ref. [79], in comparison with the power density in the SQ limit for the respective band gaps. The graph illustrates the losses when going from the power contained in the spectrum first to the SQ limit (caused by thermalization, recombination, and transmission of photons below the band gap) as well as further losses when going from the SQ limit to the real devices cause mostly due to the V_{oc}FF product in the real cell always being a bit lower than in the SQ limit due to additional nonradiative recombination processes.

and due to a decrease in the V_{oc}FF product due to additional nonradiative recombination processes.

In order to quantify these losses between the SQ limit (with a step-function-like absorptance) and the radiative limit (with an arbitrarily shaped absorptance or quantum efficiency), we would need to have a way to decide which band gap should be used for calculating the SQ limit even in situations where the definition of a band gap might be less straightforward as for crystalline semiconductors.

3.1. Defining a Photovoltaic Band Gap

One approach to find a universal band gap definition inspired by photovoltaic functionality is described in ref. [80]. The idea is to interpret a given realistic (nonstep-function-like) quantum efficiency, as shown in **Figure 4**a, required for Equations (10) and (11) as a sum over many step functions $H(E)$, that is

$$Q_e^{PV}(E) = \int_{-\infty}^{\infty} P(E_g)H(E - E_g)dE_g \tag{12}$$

where P is a distribution function. We may also write

$$\frac{d}{dE}Q_e^{PV}(E) = \int_{-\infty}^{\infty} P(E_g)\frac{d}{dE}H(E - E_g)dE_g$$
$$= \int_{-\infty}^{\infty} P(E_g)\delta(E - E_g)dE_g = P(E) \tag{13}$$

i.e. the band gap distribution equals the derivative of the external quantum efficiency $Q_e^{PV}(E)$ with respect to the photon energy as shown in Figure 4b.

In ref. [80], we suggested to define the photovoltaic band gap energy E_g^{PV} as the mean peak energy of the distribution $P(E_g)$ via[80]

$$E_g^{PV} = \int_a^b E_g P(E_g)dE_g \Big/ \int_a^b P(E_g)dE_g \tag{14}$$

We chose the integration limits a and b as the energy (close to the absorption edge at low energies) where $P(E_g)$ is equal to 50% of its maximum, $P(a) = P(b) = \max[P(E_g)]/2$. Note that for the purpose of calculating E_g^{PV} it is important to avoid the high-energy edge where the photovoltaic quantum efficiency typically decreases toward the UV part of the spectrum.

3.2. Thermodynamic Limits of the Open-Circuit Voltage

The method for defining a photovoltaic band gap described above allows us to study the difference

$$V_{oc,SQ} - V_{oc,rad} = \frac{kT}{q}\ln\left(\frac{J_{sc,SQ}}{J_{0,SQ}}\right) - \frac{kT}{q}\ln\left(\frac{J_{sc}}{J_{0,rad}}\right)$$
$$= \frac{kT}{q}\ln\left(\frac{J_{sc,SQ}}{J_{sc}} \times \frac{J_{0,rad}}{J_{0,SQ}}\right) \tag{15}$$

in the open-circuit voltage between the SQ limit and the radiative limit with an arbitrary absorptance or quantum efficiency. The equations for the different terms in Equation (15) can be found in Equations (1), (4), (10), and (11). Thus, when going from the SQ case to the radiative case for the open-circuit voltage, we obtain two loss terms, one describing the decrease in short-circuit current and the other describing the increase in the saturation current density. Both effects are due to the change from a step-function-like quantum efficiency to an experimentally measured quantum efficiency. If we now allow for nonradiative recombination to happen, we may extend this methodology to the actually measured open-circuit voltage. We may split up the voltage loss[80,81]

$$V_{oc,SQ} - V_{oc} = \frac{kT}{q}\ln\left(\frac{J_{sc,SQ}}{J_{0,SQ}}\right) - \frac{kT}{q}\ln\left(\frac{J_{sc}}{J_0}\right)$$
$$= \frac{kT}{q}\ln\left(\frac{J_{sc,SQ}}{J_{sc}} \times \frac{J_{0,rad}}{J_{0,SQ}} \times \frac{J_0}{J_{0,rad}}\right)$$
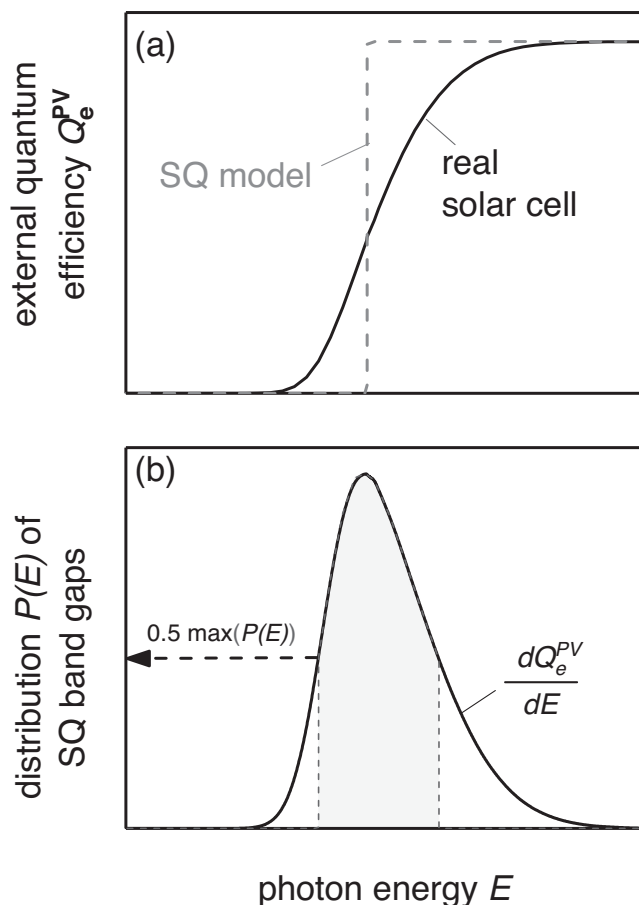$$= \Delta V_{oc,sc} + \Delta V_{oc,rad} + \Delta V_{oc,nrad} \tag{16}$$

Figure 4. For the purpose of open-circuit voltage loss analyses, we propose to a) use the inflection point of the photovoltaic quantum efficiency $Q_e^{PV}(E)$. b) The first derivative of the photovoltaic quantum efficiency $Q_e^{PV}(E)$ with respect to energy that we interpret as a distribution of SQ-type band gaps. We determined the band gap of experimental data not by using the maximum of the function shown in panel (b) but (to avoid noise), we determined the mean energy value of the shaded region (50% of the maximum value of $P(E)$ before and after the peak) as defined by Equation (14). Reproduced with permission.[80] Copyright 2017, American Physical Society.

into the two terms ($\Delta V_{oc,sc}$, $\Delta V_{oc,rad}$) discussed above and a final term due to nonradiative recombination ($\Delta V_{oc,nrad}$). It is, in particular, this third term that is typically limiting the open-circuit voltage of solar cells and often also their power conversion efficiencies. The loss $\Delta V_{oc,nrad}$ is related to the external light-emitting diode (LED) quantum efficiency Q_e^{lum} and is often[75,82,83] written in the form

$$V_{oc} = V_{oc,rad} + \frac{kT}{q}\ln\left(\frac{J_0^{rad}}{J_0}\right)$$
$$= V_{oc,rad} + \frac{kT}{q}\ln\left(Q_e^{lum}\right) \quad (17)$$

Figure 5 is an example of the application of the above-described methodology to split up the voltage losses of specific solar cells into three parts: $\Delta V_{oc,sc}$ due to a loss in short-circuit
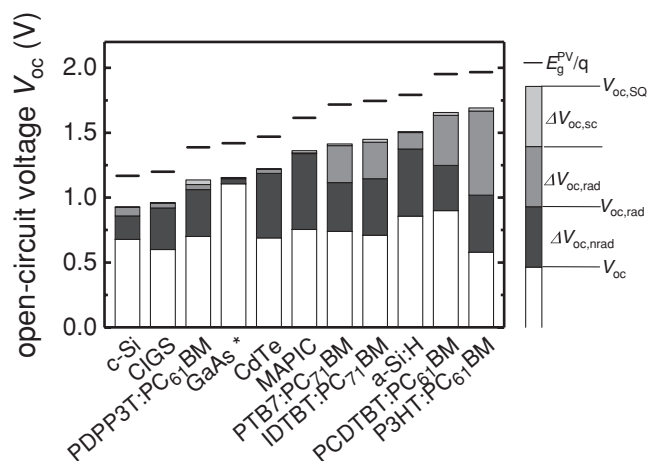

Figure 5. Comparison of the three different types of open-circuit voltage losses, namely $\Delta V_{oc,sc}$ due to a loss in short-circuit current density (light gray), the loss $\Delta V_{oc,rad}$ due to the shape of the quantum efficiency leading to radiative recombination below the SQ gap, and $\Delta V_{oc,nrad}$ due to nonradiative recombination. These losses are shown for various specific solar cells whose data were published in refs. [80,81,84–87]. Note that the cells are not (necessarily) record efficiency cells. Adapted with permission.[80] Copyright 2017, American Physical Society.

current density (light gray), $\Delta V_{oc,rad}$ due to the shape of the quantum efficiency leading to radiative recombination below the SQ gap, and $\Delta V_{oc,nrad}$ due to nonradiative recombination. Note that the data used for Figure 5 are obtained from specific solar cells that are not necessarily the record solar cells in the field. A similar analysis on record solar cells taken, e.g., from the photovoltaic efficiency tables has been done,[84] but is hampered by the absence of electroluminescence data for most cells in the photovoltaic efficiency tables.[24]

4. Connecting Internal and External Parameters

While the extension of the detailed balance approach to externally measurable quantities such as the external photovoltaic and the external LED quantum efficiency[75] has proven to be useful in terms of analyzing experimental data, this approach does not allow us to analyze the effect of internal material parameters directly. Especially, for purposes of studying the potential of a certain material rather than a device, we need to be able to calculate efficiencies from internal material parameters such as absorption coefficient or internal luminescence quantum efficiency rather than their external counterparts absorptance and external luminescence quantum efficiency. Here, we have essentially two options of how to proceed. Because we do not consider finite mobilities yet, there is no need at this point to already use drift–diffusion solvers that solve the continuity equations for electrons and holes and the Poisson equation. If we want to relate the achievable efficiency in the limit of high mobilities to the internal luminescence quantum efficiency, we need an optical model both for the determination of the short-circuit current and for the determination of the recombination current. However, if we want to relate the efficiency to the lifetime or recombination

**ADVANCED
SCIENCE NEWS**

www.advancedsciencenews.com

**ADVANCED
ENERGY
MATERIALS**

www.advenergymat.de

coefficient for nonradiative recombination, the calculation of the recombination current is substantially simpler. We will discuss both approaches in the following, starting with the one that expresses the recombination current as a function of the internal luminescence quantum efficiency.

4.1. Absorption Coefficient versus Absorptance

Relating the efficiency in the high-mobility limit to the absorption coefficient and the internal luminescence quantum efficiency requires an optical model and the complex refractive index, consisting of a real part (n_r) and an imaginary part, which is also called the extinction coefficient k. The extinction coefficient is related to the absorption coefficient via $k = \alpha\lambda/(4\pi)$, where λ is the wavelength of light, i.e., one may express the equations of the optical models using either k or α. In the following, we will use α, because it is typically used in the context of simple analytical models as the ones discussed below.

First, we have to connect absorption coefficient α and (the real part of the) refractive index n_r with the absorptance. Especially for thin-film solar cells, optical models may have to be quite sophisticated if they are supposed to accurately describe the absorptance of a photovoltaic absorber layer including the effect of light scattering and interferences. In order to illustrate the principle, however, quite simple models are sufficient. As already done in previous publications,[88,89] we choose the two configurations shown in **Figure 6**. In both cases, we assume that the front surface features a good antireflective coating, so we can ignore reflection at the front contact. In addition, we assume a perfect mirror on the backside and ignore all interferences. In such a situation, two generic situations remain. The one shown in Figure 6a) is the idealized Lambert–Beer case with the absorptance given by

$$a_{LB} = 1 - \exp(-2\alpha d) \tag{18}$$

with d being the absorber layer thickness. Note that a_{LB} is independent of refractive index n_r. Figure 6b illustrates the case with a perfect Lambertian scatterer at the front. There are several equations that more or less precisely describe the absorptance in such a situation.[91] A popular approximation is[90]

$$a_{LT} = \left(1 + \left[4n_r^2\alpha d\right]^{-1}\right)^{-1} \tag{19}$$

Using $J_{sc} = q\int_0^\infty a\phi_{sun}(E)dE$, the knowledge of the absorptance is enough to calculate J_{sc} if we assume collection is efficient.

As mentioned above, we could calculate V_{oc} and the photovoltaic efficiency, if we knew the "external" luminescence quantum efficiency. If we only have information on material parameters describing recombination, such as radiative or nonradiative lifetimes, trap densities, or internal luminescence quantum efficiencies, we also need an optical model to calculate solar cell efficiency. Before we discuss the relation between internal and external luminescence quantum efficiencies, we will, however, first introduce and define nonradiative and radiative recombination rates and lifetimes.

4.2. External versus Internal Luminescence Quantum Efficiency

The Shockley–Read–Hall (SRH) recombination[92,93] rate

$$R_{SRH} = \frac{np - n_0 p_0}{(n + n_1)\tau_p + (p + p_1)\tau_n} \tag{20}$$

is used to describe recombination via defect levels in the band gap. Here, we use the abbreviations $n_1 = N_C \exp[(E_T - E_C)/kT]$ and $p_1 = N_V \exp[(E_V - E_T)/kT]$, where E_T is the trap level. Thus, n_1 and p_1 are small for deep traps but become important once the trap level is close to the conduction band (n_1 becomes large) or close to the valence band (p_1 becomes large). Note that SRH recombination is strictly suited only for singly charged defects (0/−) or (+/0) while the so-called Sah–Shockley statistics[94,95] is designed to describe recombination via amphoteric defects (+/0/−) such as dangling bonds in Si. However, for the purpose of this review we restrict ourselves to the description of recombination via traps using SRH statistics. This type of recombination is typically the dominant nonradiative recombination mechanism in most solar cell materials. The other nonradiative recombination mechanism is Auger recombination which is of particular relevance for crystalline Si at high doping densities or high injection conditions (high voltages or high light intensities).[96–98] In the following, we will just consider SRH recombination in relation to the radiative recombination rate
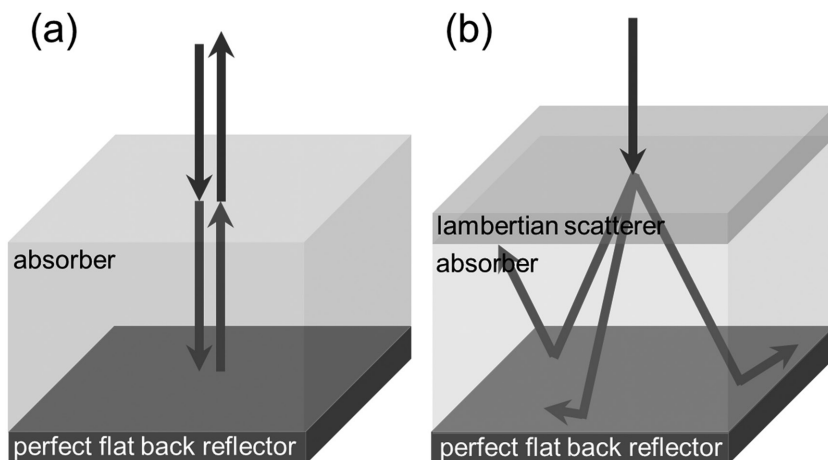

Figure 6. Schematic of the two optical models described in a) Equation (18) and b) Equation (19). Panel (a) illustrates a situation, where we consider ray optics, perfect light incoupling, and a perfect back reflector but no scattering. The absorptance is described for direct incidence by an equation (Equation (18)) based on Lambert–Beer's law. The situation shown in panel (b) considers a perfect Lambertian scattering layer that leads to a Lambertian distribution of angles which is frequently used for efficiency limit calculations[88,90] for instance for crystalline Si. Adapted with permission.[88] Copyright 2016, American Chemical Society.

ADVANCED
SCIENCE NEWS
www.advancedsciencenews.com

ADVANCED
ENERGY
MATERIALS
www.advenergymat.de

that was implicitly already considered in the Shockley–Queisser limit. Implicitly means here that for the Shockley–Queisser limit, the radiative recombination rate does not have to be explicitly calculated but instead it only requires calculating the radiative recombination current (cf. Equations (4) and (11)). Just as the radiative recombination current follows from the absorptance (or quantum efficiency) of the solar cell, the radiative recombination rate is linked to the absorption coefficient α (i.e., the internal parameter governing absorption). We can write down the detailed balance condition for radiative recombination by equating the rates for recombination and absorption in equilibrium which leads to[99]

$$k_{rad}n_i^2 = \int_0^\infty 4\alpha n_r^2\phi_{bb}\,dE \tag{21}$$

where k_{rad} is the radiative recombination coefficient. The radiative recombination rate is then $R_{rad} = k_{rad}(np - n_i^2)$. We have shown in Section 3 (Equation (17)), the open-circuit voltage of a solar cell is directly related to the external luminescence quantum efficiency Q_e^{lum} which relates radiative and total recombination "currents."[75] The equivalent internal quantity is the internal luminescence quantum efficiency Q_i^{lum}, which is defined as the ratio of the radiative to total recombination "rates" rather than currents. Thus

$$Q_i^{lum} = \frac{R_{rad}}{R_{rad} + R_{SRH}} = \frac{k}{k_{rad} + \dfrac{1}{(n+n_1)\tau_p + (p+p_1)\tau_n}} \tag{22}$$

Note that Q_i^{lum} is a function of n and p, and therefore it may change with voltage (in case of electroluminescence) or laser intensity (in case of photoluminescence).

The relation between internal and external luminescence quantum efficiencies depends on the fate of the photon that is created by radiative recombination. There are three options we need to distinguish: the photon may be emitted with probability p_e; it may be parasitically absorbed with probability p_a; or it may be reabsorbed with probability p_r and create a new electron–hole pair thereby starting the process again.[100] The sum of the three probabilities has to be one, i.e., $p_e + p_a + p_r = 1$. The radiative recombination rate will cause an internal generation rate $G_{int} = p_r R_{rad}$ that is due to the solar cell illuminating itself. Thus, the effective recombination current density including G_{int}, R_{rad}, and R_{SRH} is

$$J_{rec} = q\int_0^d (R_{SRH} + R_{rad} - G_{int})\,dx$$
$$= q\int_0^d (R_{SRH} + [1 - p_r]R_{rad})\,dx \tag{23}$$

If we now assume for simplicity that G_{int}, R_{rad}, and R_{SRH} are constant everywhere in the device, we obtain[101]

$$J_{rec} = qd[R_{SRH} + (1 - p_r)R_{rad}] \tag{24}$$

Under the same assumption, the radiative recombination current density expressed as a function of R_{rad} is given by

$$J_{rad} = qdp_eR_{rad} \tag{25}$$

and finally the external luminescence quantum efficiency is[88,101]

$$Q_e^{lum} = \frac{J_{rad}}{J_{rec}} = \frac{p_eR_{rad}}{R_{SRH} + (1 - p_r)R_{rad}}$$
$$= \frac{p_eQ_i^{lum}}{1 - p_rQ_i^{lum}} = \frac{p_eQ_i^{lum}}{(1 - Q_i^{lum}) + (p_e + p_a)Q_i^{lum}} \tag{26}$$

where we used the definition of Q_i^{lum} given by Equation (22). If we insert Equation (26) in Equation (17), we directly obtain the relation

$$qV_{oc} = qV_{oc}^{rad} + kT\ln\{Q_e^{lum}\}$$
$$= qV_{oc}^{rad} + kT\ln\left\{\frac{p_eQ_i^{lum}}{(1 - Q_i^{lum}) + (p_e + p_a)Q_i^{lum}}\right\}$$
$$= qV_{oc}^{rad} + kT\ln\left\{\frac{p_eQ_i^{lum}}{1 - p_rQ_i^{lum}}\right\} \tag{27}$$

between the open-circuit voltage V_{oc} and the internal quantum efficiency Q_i^{lum}.

Based on our analysis so far, we conclude that an optical model and optical material properties are necessary to calculate the absorptance and subsequently also the J_{sc} (Equation (10)). In addition, both are necessary to calculate V_{oc} from the internal luminescence quantum efficiency Q_i^{lum} or any V_{oc} close to the radiative limit where R_{rad} is not $\ll R_{SRH}$. In contrast, the dark recombination current away from the radiative limit, i.e., $J_{rec} = q\bar{R}_{SRH}d$, is accessible without any knowledge about optical parameters or optical models.

The calculation of V_{oc} from Q_i^{lum} requires the knowledge of how many photons are coupled out, reabsorbed, or parasitically absorbed. While the outcoupling efficiency follows directly from the absorptance a and the absorption coefficient α via[101]

$$p_e = \frac{\int_0^\infty a\phi_{bb}\,dE}{\int_0^\infty 4\alpha\,dn_r^2\phi_{bb}\,dE} \tag{28}$$

it is not straightforward to discriminate between reabsorption and parasitic absorption. A quantitative discrimination between p_a and p_r requires calculating the absorption of photons emitted by point sources distributed over the depth of the solar cell absorber.

In **Figure 7** we illustrate the effect of parasitic absorption on the loss in open-circuit voltage relative to the radiative limit for a given value of (a) $Q_i^{lum} = 1$ and (b) $p_e = 5\%$. We use two y-axes, with the left one being the voltage loss relative to the radiative limit and the right one being the external luminescence quantum efficiency. Figure 7a illustrates the case, where there is only radiative recombination in the absorber layer; however, not all of the light is outcoupled or reabsorbed in the absorber. Instead, a certain percentage p_a of photons are lost by parasitic absorption, e.g., in a contact layer
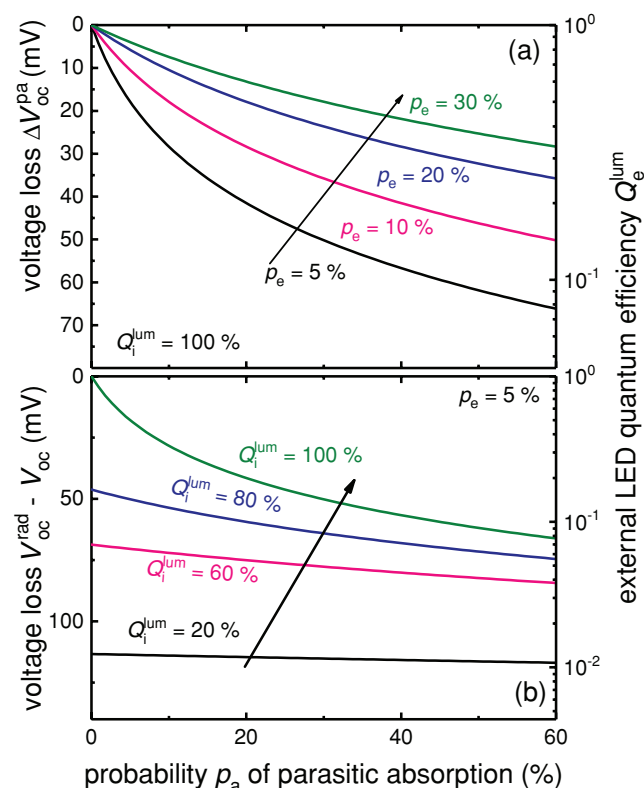
**ADVANCED
SCIENCE NEWS**
www.advancedsciencenews.com

**ADVANCED
ENERGY
MATERIALS**
www.advenergymat.de

Figure 7. a) Open-circuit voltage loss due to parasitic absorption as a function of the probability p_a of parasitic absorption in the radiative limit ($Q_i^{lum} = 1$). b) Total open-circuit voltage loss $V_{oc}^{rad} - V_{oc}$ as a function of p_a and Q_i^{lum} assuming a constant emission probability $p_e = 5\%$. Adapted with permission.[88] Copyright 2016, American Chemical Society.

where they do not create a long-lived electron–hole pair that would contribute to V_{oc}. The loss in this situation is given by $Q_e^{lum} = \exp(-q\Delta V_{oc}^{pa}/kT) = p_e/(p_e + p_a)$ and, thus, becomes less relevant the higher the outcoupling efficiency p_e is.

Figure 7b illustrates the case, where the outcoupling efficiency is constant, but Q_i^{lum} is varied. For high values of Q_i^{lum}, the effect of parasitic absorption is quite strong, while for values $Q_i^{lum} \leq 20\%$, photon recycling has only a weak effect on V_{oc} and therefore parasitic absorption becomes irrelevant for V_{oc}. However, it may still be relevant for J_{sc}.

Based on the equations discussed in Sections 4.1 and 4.2, we can calculate the current–voltage curve under illumination as $J = -J_{sc} + J_{rec}$ and the power density as $P = -JV$. From the maximum of the power density as a function of voltage, we then obtain the efficiency as discussed already in Section 2.

4.3. Efficiency as a Function of the Absorption Coefficient and Lifetime

If we want to calculate the high-mobility limit to efficiency as a function of the absorption coefficient and the lifetime of charge carriers, we may use the previously introduced Equation (10) to calculate J_{sc}, and Equation (11) to calculate $J_{0,rad}$. In order to calculate the recombination current, it is useful to study to extreme situations. The first scenario describes the situation

where recombination is dominated by recombination in the neutral zone of a p–n-junction solar cell, i.e., where one type of carrier is present in excess of the other (i.e., $n \ll p$ or $p \ll n$). This situation is called low-level injection. In low-level injection, the recombination rate $R = \Delta n/\tau$. In the high-mobility limit, the recombination current corresponding to this rate is $J = qRd$. The saturation current density is the recombination current in thermal equilibrium, that is

$$J_0^{low} = qd\frac{n_0}{\tau} = qd\frac{N_C N_V}{N_d \tau}\exp\left(\frac{-E_g}{kT}\right) \tag{29}$$

where N_C and N_V are the effective density of states of the conduction and valence band, N_d is the doping density, $\tau = \tau_n = \tau_p$.

The second scenario that may be easily treated analytically is when we assume the solar cell absorber layer to be fully depleted with electron and hole concentrations being similar (i.e., $n \approx p$). In this case, the saturation current density under high injection conditions is given by

$$J_0^{high} = qd\frac{\sqrt{N_C N_V}}{2\tau}\exp\left(\frac{-E_g}{2kT}\right) \tag{30}$$

which is a process with an ideality of 2. Thus the voltage-dependent recombination current in this case reads

$$J_{SRH}^{high} = J_0^{high}\left[\exp\left(\frac{qV}{2kT}\right) - 1\right] \tag{31}$$

Note that Equations (29)–(31) neglect surface recombination for the sake of an analytical treatment. The saturation current densities introduced in Equations (29) and (30) depend linearly on thickness with higher thicknesses leading to a larger volume where recombination may take place and, therefore, a higher value of J_0. The total current voltage curve then follows as

$$J = -J_{sc} + J_0^{low/high}\left[\exp\left(\frac{qV}{n_{id}kT}\right) - 1\right] + J_{0,rad}\left[\exp\left(\frac{qV}{kT}\right) - 1\right] \tag{32}$$

where the ideality factor $n_{id} = 1$ for low injection and $n_{id} = 2$ for high injection. From the current–voltage curve we can obtain the efficiency as discussed before using Equation (7).

4.4. The Optimum Thickness in the High-Mobility Limit

When comparing material parameters like absorption coefficient α and Q_i^{lum} or the SRH lifetime τ, it is important to understand their relative importance. The importance of absorption relative to recombination will depends on the chosen thickness of the assumed device. When we assume, for instance, a rather small thickness, increasing the absorption coefficient might be highly beneficial. In contrast, for a larger thickness, absorption will already have saturated, but reducing the amount of recombination will now be of more important. Thus, this does not seem to be a simple relation linking α and τ with the efficiency at an arbitrary thickness. However, if nonradiative recombination is dominant, efficiency will always have an optimum value as a function of thickness. The short-circuit current density will increase with
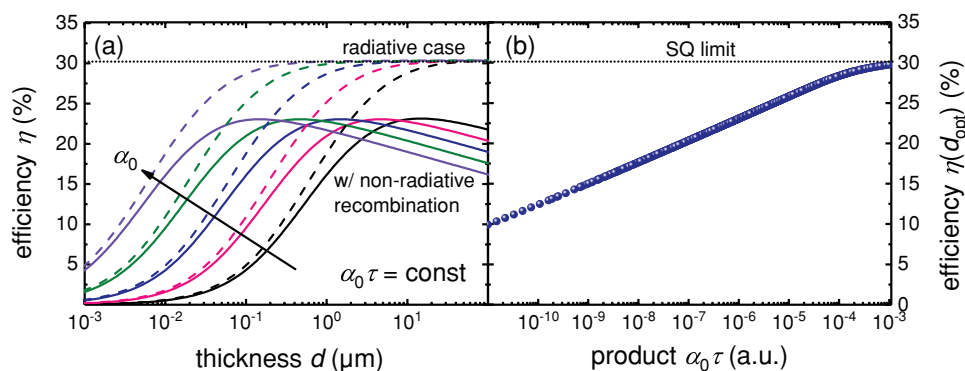
Figure 8. a) Efficiency as a function of thickness assuming infinite mobilities and therefore perfect charge collection, a direct band gap ($E_g = 1.6$ eV) with an absorption coefficient given by $\alpha = \alpha_0 \sqrt{(E - E_g)/kT}$ and radiative (dashed lines) as well as radiative and nonradiative recombination (solid lines). The saturation current density for nonradiative recombination is assumed to increase linearly with thickness. As long as nonradiative recombination is dominant, the maximum efficiency hardly changes as long as $\alpha_0 \tau$ is constant. b) Efficiency η at the optimum thickness as a function of the product $\alpha_0 \tau$, when varying α_0 and τ over a wide range. The efficiency depends only on the product $\alpha_0 \tau$ with higher $\alpha_0 \tau$ leading to higher efficiencies. As long as the efficiency is not saturated because it approaches the SQ limit for high $\alpha_0 \tau$, the efficiency scales linearly with $\ln(\alpha_0 \tau)$.

thickness until a saturation value is reached where absorption above the band gap is efficient. If we assume efficient collection, J_{sc} will then remain constant for higher thickness. In contrast, the open-circuit voltage in the radiative limit will decrease with thickness[88,89,102] because J_0 increases faster with thickness (linearly) than J_{sc} (sublinearly). Therefore, the product J_{sc}–V_{oc} and consequently also the efficiency will have a peak at a finite thickness even in the limit of infinite mobilities. The optimum thickness is strongly coupled to the absorption coefficient with higher values of α leading to lower optimum thicknesses. Interestingly, the efficiency $\eta(d_{opt})$ at the optimum thickness d_{opt} in a simple model as described in ref. [89] is directly related to the product $\alpha_0 \tau$, if we assume, for instance, $\alpha = \alpha_0 \sqrt{(E - E_g)/kT}$. We are not aware of a simple analytical derivation of this relation but it is easy to illustrate this relation graphically. **Figure 8**a shows the efficiency calculated as a function of thickness in the limit of high mobilities for four sets of parameters that are different with respect to the prefactor α_0 of the absorption coefficient and the SRH lifetime τ. We observe that as long as the product of the two is kept constant, the maximum efficiency remains constant. The higher α_0 and the lower τ are, the lower the optimum thickness will be.

Figure 8b presents the optimum efficiency calculated using the J–V curves as given by Equation (32) as a function of optimum thickness if the prefactor α_0 of the absorption coefficient and the SRH lifetime τ are varied over a large parameter range. This shows the robustness of the observation from Figure 8a. We also observe that the efficiency is proportional to $\ln(\alpha_0 \tau)$ over a large range of parameters. Only for very high $\alpha_0 \tau$ products, the efficiency goes into the saturation defined by the SQ limit.

5. Charge Collection and Electrostatics

So far we have discussed the effect of optical properties of the material as well as recombination on photovoltaic efficiency in the limit where charge collection and charge transport are efficient. Because the quasi-Fermi levels will be flat in the limit of high mobilities (whereby the definition of "high" depends on

the thickness of the device), we are still able to use analytical equations to describe the recombination currents. However, already in Section 4.3, we had to distinguish between recombination in high and low injection, i.e., we had to consider the relative width of the space-charge region relative to the total active layer thickness. If we relax the condition of infinite mobilities, we need to change the level of theory required to describe the connection between parameters like α, μ, and τ and the solar cell J–V curve. While even with finite mobilities, the neutral zone of a p–n-junction can still be described analytically using a 1D solution to the diffusion equation of minority carriers, every complete description of a solar cell including neutral zones and space-charge regions requires the solution of the continuity equations for electrons and holes as well as the Poisson equation connecting space charge with electrostatic potential.

5.1. Drift–Diffusion Simulations

The so-called drift–diffusion simulations are based on solving three coupled differential equations, namely, the Poisson equation

$$\frac{\partial^2 \varphi(x)}{\partial x^2} = -\frac{\rho(x, n, p)}{\varepsilon} \tag{33}$$

relating the electrical potential φ to the space charge ρ and the permittivity ε, and the two continuity equations for electrons

$$\frac{dn}{dt} = G_{ext}(x) + G_{int}(x, n, p) - R(x, n, p) + D_n \frac{d^2 n(x)}{dx^2} + F\mu_n \frac{dn(x)}{dx} \tag{34}$$

and holes

$$\frac{dp}{dt} = G_{ext}(x) + G_{int}(x, n, p) - R(x, n, p) + D_p \frac{d^2 p(x)}{dx^2} - F\mu_p \frac{dp(x)}{dx} \tag{35}$$

Here G_{ext} is the generation rate of electron–hole pairs due to external illumination (usually by the sun) while G_{int} is the internal generation rate due to the absorption of photons generated by radiative recombination within the device itself (i.e., due to photon recycling). The last two terms in Equations (34) and (35) describe the derivative of diffusion and drift currents with respect to position x. The diffusion term is proportional to the diffusion coefficients $D_{n,p} = \mu_{n,p}kT/q$ while the drift term is proportional to the electric field that we will denote here as F in order to distinguish it from the energy E. In order to solve these three differential equations, boundary conditions are required. Typically, the boundary conditions used are to set the difference of the electrostatic potential between cathode and anode to a fixed value depending on voltage, i.e., $\varphi(\text{cathode}) - \varphi(\text{anode}) = V_{bi} - V$, where V_{bi} is the built-in voltage. The boundary conditions for the charge densities are typically defined such that the current for electrons or holes at cathode or anode is proportional to the respective density of electrons or holes multiplied with a constant factor called the surface recombination velocity S. Because there are four boundary conditions for charge density (electron and hole × anode and cathode), there are also four different surface recombination velocities. The surface recombination velocities for majority carriers should always be high to ensure current flow out of the right contact and the ones for minority carriers should be low to ensure that no unwanted recombination takes place at the electrodes.

While drift–diffusion simulations are widely used in the different photovoltaic communities, they rather infrequently include the G_{int} term in Equations (34) and (35). This is due to the fact that it is complicated and time consuming to calculate the interaction of every coordinate in the device (where radiative recombination could take place) with every other coordinate that may absorb the photon.[103,104] In addition, in many cases radiative recombination is slow relative to nonradiative recombination, i.e., $Q_i^{lum} \ll 1$ and in this case, G_{int} will be small compared to G_{ext} even at voltages around V_{oc}, where internal generation is highest. However, we want to stress that only while including the G_{int} term, the result of a drift–diffusion simulation will converge to the radiative limit for high mobilities and $Q_i^{lum} = 1$.[105] In addition, only including G_{int} into a drift–diffusion solver would allow one to study situations, where mobilities are low and charge collection might be improved by photon recycling supporting the diffusion of charge carriers by redistributing them optically. In the limit of zero mobility, charge redistribution would only proceed via a series of absorption and re-emission events, which is the situation encountered in a fluorescent collector.[63,64]

In the following, we will focus on the effect of the electric field distribution on charge collection and photovoltaic performance using drift–diffusion simulations as introduced in this section. The focus is on effects that go beyond the ones that could be described in the high-mobility limit discussed in Section 4.

5.2. Full versus Partial Depletion

In this section, we discuss the general aspects relevant for charge collection with a peculiar emphasis on the topic of electrostatics, i.e., the electric fields within the device. Solar cells typically have at least one space-charge region serving to build up a built-in voltage that helps separating charge carriers. While the built-in voltage is not a necessary prerequisite for charge separation, it does help to perform that job for a range of voltages between short circuit and open circuit.[106–108] One way of classifying solar cell geometries is therefore to study the properties of the space-charge region and, in particular, the width w of the space-charge region in the device relative to the thickness d of the whole absorber layer. In some solar cells, there may be more than one space-charge region, e.g., the p–n-junction and the p–p+ (or n–n+) junction (back surface field) in crystalline silicon solar cells. In this case, w refers to the width of the junction that makes the highest contribution to the built-in voltage (in the above example, the p–n-junction).

If we compare the typical ratio, w/d, over a range of technologies as shown in **Figure 9**a, we observe that the ratio may span several orders of magnitude. On the low end of the scale (small space-charge region relative to total active layer thickness), we have, for instance, crystalline Si solar cells but also dye-sensitized solar cells. On the high end, there are typical thin-film solar cell technologies, often those with low-mobility–lifetime products, such as amorphous Si or organic solar cells. Figure 9b,d,f shows the band diagrams of solar cells with different ratio, w/d, at $V = 0$ V in the dark with the space-charge region being highlighted. If the ratio is low (Figure 9b), most of the device is field free already at short circuit, and collection of photogenerated carriers would happen by diffusion. The space-charge region only works as a carrier selective barrier (for holes in this case). The key parameter to describe collection is then the ratio of diffusion length L_{diff} (of electrons in this example) and thickness d. The diffusion length is directly related to the mobility–lifetime product via $L_{diff} = \sqrt{\mu\tau kT/q}$. In contrast, if
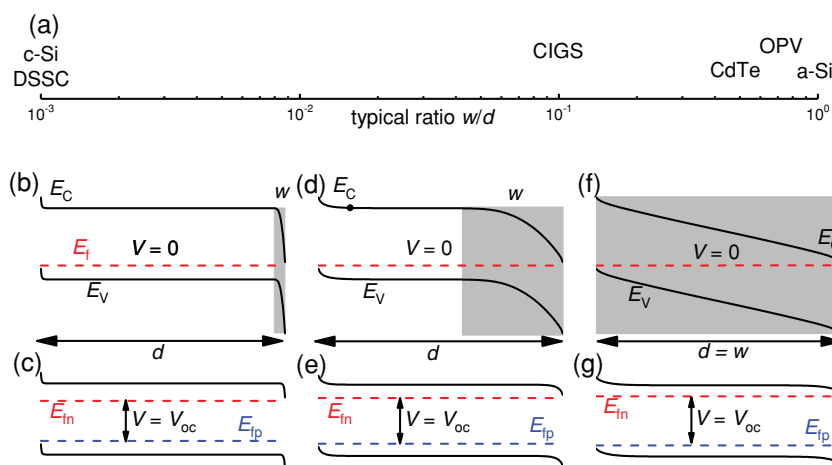

Figure 9. a) Typical ratio of the width w of the space-charge region and the absorber thickness d for various types of solar cells. b–f) Band diagrams for diodes with varying width of the space-charge region in equilibrium (upper row) and at open circuit under illumination (lower row). Reproduced with permission.[108] Copyright 2015. PCCP Owner Societies.
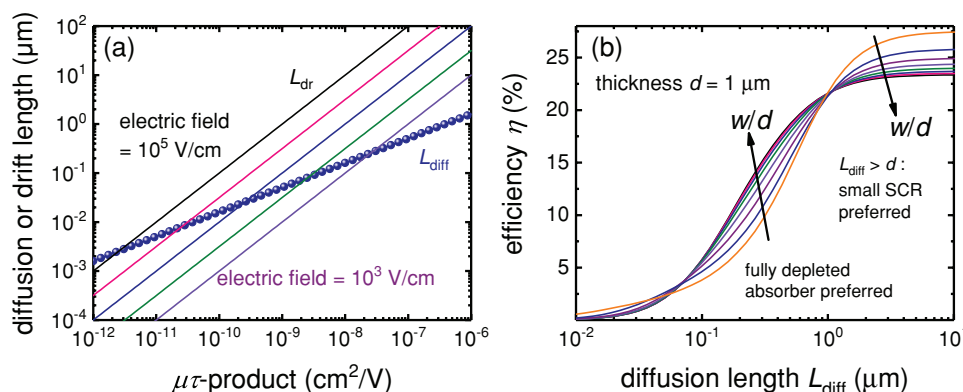
Figure 10. a) Diffusion length and drift length as a function of the mobility–lifetime product. The diffusion length $L_{diff} = \sqrt{\mu\tau kT/q}$ is shown with symbols. The drift length $L_{dr} = \mu\tau F$ is shown for different values of the electric field F. The higher the electric field, the larger the region of when $L_{dr} > L_{diff}$. b) Efficiency as a function of the diffusion length for different ratios w/d. For $L_{diff} > d$, small space-charge regions are beneficial, because regions where n and p cause higher SRH recombination and therefore lower V_{oc} and FF. For $d/10 < L_{diff} < d$ charge collection is improved by an electric field and therefore larger space-charge regions are better. For very small diffusion lengths, charge collection also in a fully depleted absorber would be inefficient. In this case, the small space-charge regions are better because collection at least in this small space-charge region is high because of the high local electric field. b) Reproduced with permission.[108] Copyright 2015. PCCP Owner Societies.

the ratio w/d approaches 1 (Figure 9f), at short circuit there is a relatively constant field separating electrons and holes. In this situation, collection of photogenerated carriers is controlled by the ratio of drift length L_{dr} and thickness d, where the drift length is defined as $L_{dr} = \mu\tau F$.

Figure 9c,e,g shows the corresponding band diagrams at open circuit. In the case with $w/d \ll 1$, the electric field remains zero in most of the device. Changes occur only in the space-charge region which takes up only a tiny part of the total volume. Thus, charge collection close to V_{oc} is still controlled entirely by diffusion and is largely independent of voltage. If collection is efficient at short circuit, it will also be efficient at open circuit. In contrast, if $w/d = 1$, collection is controlled by drift and because the drift length is proportional to the electric field, the collection efficiency might change with voltage as long as we are not in the limit of very efficient collection ($L_{dr} \gg d$). Thus, charge collection losses are often visible in the fill factor (FF) in the case of thin-film solar cells with $w/d \approx 1$ but not in thick solar cells with $w/d \ll 1$. Note that toward higher voltages close to V_{oc}, usually the electric field in a p–i–n device becomes low and inhomogeneous (high toward the contacts and lower in the middle) which makes the concept of a drift length using an average electric field problematic around V_{oc}.

Figure 10a shows the diffusion length and various drift lengths for different values of the electric field as a function of the mobility–lifetime product. We chose a double-logarithmic presentation of the data which implies that both diffusion and drift length are straight lines, albeit with a different slope. The square-root-like dependence of the diffusion length on the $\mu\tau$ product compared with the linear dependence of the drift length ensures that there is always a cross over which then depends only on temperature and electric field. Figure 10b presents the efficiency as a function of diffusion length for a 1 µm thick active layer and assuming that recombination is dominated by SRH recombination via a deep trap. The simulations were done using a drift–diffusion solver (ASA[109]) by varying the mobility while the SRH lifetime was kept constant at $\tau_n = \tau_p =$

1 µs. We varied the doping density such that the ratio w/d changed from 1 to $\ll 1$. In a range $d/10 < L_{diff} < d$, charge collection is improved by an electric field, i.e., $L_{dr} > L_{diff}$ leads to an improved efficiency for the fully depleted devices $w/d = 1$. However, for higher diffusion lengths, collection becomes efficient no matter whether drift or diffusion is dominant. In this situation, Figure 10b predicts that fully depleted devices are worse than partly depleted devices for high diffusion lengths. This reversal of the optimum doping density in this idealized toy model cannot be explained by Figure 10a and by the differences between drift and diffusion lengths. Instead, the explanation is due to the effect of doping and depletion zones on recombination close to the open-circuit voltage. Within a depletion region, the densities of electrons and holes are roughly equal, and this condition will maximize the value of R_{SRH} in Equation (20) if we assume the product np to be constant. Thus, increasing the volume where $n \sim p$ leads to faster collection but also to higher recombination at forward bias. In addition, SRH recombination in the space-charge region with $n = p$ leads to an ideality factor of 2 and thereby a reduced FF.[110,111] For these two reasons, p–n-junction solar cells are beneficial relative to pin-junction solar cells in situations, where (i) SRH recombination is dominant, (ii) doping does not (strongly) deteriorate SRH lifetimes, and (iii) charge collection is already efficient due to sufficiently high mobilities.

6. Relations between Microscopic Material Parameters and α, μ, and τ

So far we have learned how to calculate solar cell efficiency based on external parameters such as the external solar cell and luminescence quantum efficiency as well as on material parameters such as absorption coefficient α, charge-carrier mobility μ, and lifetime τ. The final step, necessary for an explanation of an already discovered suitability for photovoltaics or alternatively the identification of new materials for photovoltaics,

**ADVANCED
SCIENCE NEWS**

www.advancedsciencenews.com

**ADVANCED
ENERGY
MATERIALS**

www.advenergymat.de

requires finding relations between α, μ, and τ and microscopic parameters such as the band structure or the phonon energies. Many microscopic parameters such as the effective mass have an impact on all three parameters, and it may not be obvious whether, for instance, the increase in absorption for higher effective masses is counterbalanced by an increase in recombination and a decrease in mobility. Thus, there is no need to look at the quantities α, μ, and τ separately. Rather we must consider the combined effect of microscopic parameters on all three quantities. While there is no simple equation that connects efficiency η to α, μ, and τ, empirically such relations can be found as shown in Section 4.2. For instance, if we assume mobility to be high and the absorption coefficient to be described by $\alpha = \alpha_0 \sqrt{(E - E_g)/kT}$, the efficiency at the optimum thickness will depend on the product $\alpha_0 \tau$. In the following, we will therefore briefly review analytical relations between α and τ and microscopic properties, e.g., of the semiconductor crystal for the case of an inorganic semiconductor. In a later stage, we will compare our findings to the situation in organic semiconductors used for photovoltaics.

6.1. Absorption Coefficient and Effective Mass

Simple relations between the absorption coefficient and microscopic parameters such as the effective mass are given, for instance, by Ridley who expresses the absorption coefficient α_{dir} for interband transitions in a direct band gap semiconductor as[112]

$$\alpha_{dir} = \frac{2}{3} \alpha_{fine} a_H^2 \left(\frac{R_H}{E} \right) \frac{E_g (1 + m/m_{eff})}{n_r} \left(\frac{m_{eff}}{\hbar^2} \right)^{3/2} \sqrt{E - E_g} \tag{36}$$

Ridley uses the following abbreviations: the fine-structure constant (dimensionless) $\alpha_{fine} = q^2/4\pi\varepsilon_0\hbar c = 7.297 \times 10^{-3}$, the Bohr radius $a_H = 4\pi\varepsilon_0\hbar^2/mq^2 = 5.292 \times 10^{-11}$ m, and the Rydberg energy $R_H = q^2/8\pi\varepsilon_0 a_H = 13.605$ eV. Inserting all numerical constants into the equation leads to

$$\alpha_{dir} = \alpha_{00} \frac{E_g (1 + m/m_{eff})}{E n_r} \left(\frac{m_{eff}}{m} \right)^{3/2} \sqrt{E - E_g} \tag{37}$$

with $\alpha_{00} = 2/3 \times \alpha_{fine} a_H^2 R_H m^{3/2} \hbar^{-3} = 8.77 \times 10^4$ cm^{-1} eV$^{-1/2}$. Here m is the free electron mass ($m = 9.109 \times 10^{-31}$ kg), m_{eff} is the absolute effective mass of electrons in the conduction band and holes in the valence band (assumed equal), and $\hbar$ is the reduced Planck's constant ($\hbar = 6.582 \times 10^{-16}$ eV s).

6.2. Multiphonon Recombination and the Energy Gap Law

There are various attempts to express the recombination rate, the capture cross section, or the SRH lifetime as a function of microscopic properties of the material.[113–118] In textbooks on semiconductor devices,[119] the SRH lifetimes $\tau_{n,p}$ as introduced in Equation (20) are expressed as

$$\tau_{n,p} = \frac{1}{\sigma_{n,p} v_{th} N_t} \tag{38}$$

where $v_{th} = \sqrt{8kT/\pi m_{eff}}$ is the thermal velocity, N_t is the trap density, and $\sigma_{n,p}$ are the capture cross sections for electrons and holes. If we use the equations provided by Markvart, the lifetime for transitions involving multiple phonons (of the same type) is[120]

$$\tau = \tau_0 \left(\frac{N_t}{\sqrt{p\sqrt{1+x^2}}} \exp\left[p\left(\frac{E_{ph}}{2kT} + \sqrt{1+x^2} - x\cosh\left(\frac{E_{ph}}{2kT}\right) - \ln\left(\frac{1+\sqrt{1+x^2}}{x}\right) \right) \right] \right)^{-1} \tag{39}$$

where τ_0 is a prefactor and E_{ph} is the phonon energy. The parameter x is a function of the number p of phonons involved in the transition and the Huang–Rhys factor S_{HR} and can be expressed as

$$x = \begin{cases} \dfrac{S_{HR}}{p\sinh\left(E_{ph}/2kT\right)} & \text{for} \quad S_{HR} < p \\[2ex] \dfrac{p}{S_{HR}\sinh\left(E_{ph}/2kT\right)} & \text{for} \quad S_{HR} > p \end{cases} \tag{40}$$

The Huang–Rhys factor describes the strength of the electron–phonon coupling and contains two terms,[115] both of which decrease with phonon energy. The first term describes polar coupling and is high if the factor $(\varepsilon_\infty^{-1} - \varepsilon^{-1}(f=0))$ is high, where $\varepsilon(f)$ is the permittivity as a function of frequency f. The second term depends on the deformation coupling constant of the phonon mode. Thus, if multiphonon transitions via optical phonons are dominant, also the deformation potential constant for optical phonons is required to calculate the Huang–Rhys factor. Note that the lifetime given by Equation (39) is the lifetime for capture into a neutral state. Transitions involving attractive or repulsive defect states require multiplication of the rate with the so-called Sommerfeld factors described, e.g., in refs. [121,122].

Here, we will not go into the depths of the theory of multiphonon recombination but rather illustrate its implications for a few simple situations. We use Equation (39) with a τ_0 chosen based on ref. [123] and a completely arbitrarily chosen trap density of $N_t = 10^{15}$ cm^{-3}. We use an effective mass $m_{eff} = m$ and a relative permittivity of $\varepsilon_r = 10$ for the calculations. **Figure 11**a,b shows the resulting lifetime as a function of the energy difference between the two states involved in the multiphonon transition. These could be, e.g., the conduction band and a defect state in the band gap. Figure 11a shows the trend with phonon energy at a constant Huang–Rhys factor ($S_{HR} = 10$) and Figure 11b the trend with Huang–Rhys factor assuming a constant phonon energy ($E_{ph} = 30$ meV). Both panels are meant to illustrate the idea of the energy-gap law, which implies that higher energy differences between the two states involved in the multiphonon transition lead to slower nonradiative recombination, i.e., longer lifetimes. Note that the lifetime given by Equation (39) is the lifetime for a transition from band to defect. This is the same definition as the lifetimes τ_n and τ_p in Equation (20). Detrapping may slow down recombination for shallow traps, which is taken into account in the classical SRH statistics by the terms n_1 and p_1 in Equation (20). The effect of detrapping is therefore not taken into account in Equation (39) and Figure 11.

ADVANCED
SCIENCE NEWS
www.advancedsciencenews.com

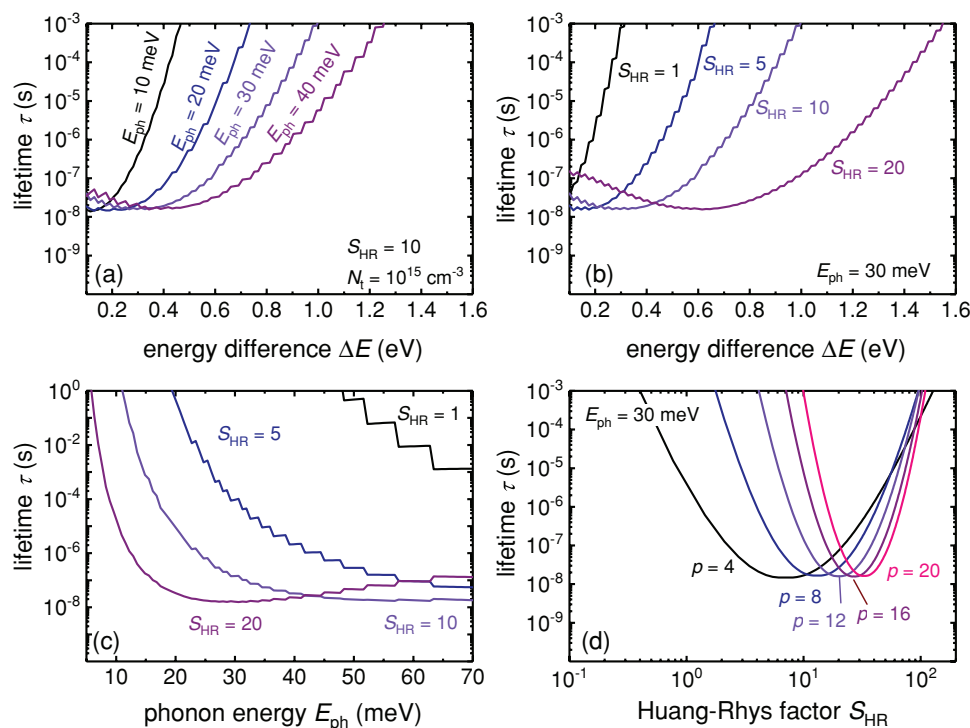ADVANCED
ENERGY
MATERIALS
www.advenergymat.de

Figure 11. Lifetime for multiphonon recombination as a function of the energy difference between ground state and excited state with a) constant Huang–Rhys factor ($S_{HR} = 10$) and varying phonon energy and b) constant phonon energy ($E_{ph} = 30$ meV) and varying Huang–Rhys factor. Note that the discrete jumps in the curves are due to the integer number of phonons needed for a transition. c) Lifetime as a function of phonon energy for constant energy difference $\Delta E = 600$ meV and varying Huang–Rhys factor. d) Lifetime as a function of Huang–Rhys factor with a constant phonon energy (30 meV) and a varying energy difference. In order to calculate the lifetime, we used an arbitrary trap density of $N_t = 10^{15}$ cm^{-3}. The minimum of the lifetime as a function of S_{HR} and the number $p = \Delta E/E_{ph}$ of phonons needed is roughly at $S_{HR} = p$. As long as $p \gg S_{HR}$, higher values of p increase lifetimes substantially. This increase in p can either be achieved by increasing the energy difference between the two states (energy gap law) or by reducing the phonon energy.

Figure 11a shows that for a constant value of the Huang–Rhys factor S_{HR}, this energy difference scales with the assumed value of E_{ph}, i.e., the number $p = \Delta E/E_{ph}$ of phonons needed for the transition has a strong effect how long the lifetime would be. If p and the Huang–Rhys factor S_{HR} are identical, the energy barrier that has to be overcome for recombination to happen is zero, and the lifetime will have a minimum value as a function of ΔE. For recombination to happen via a defect state, two transitions are needed, i.e., conduction band to defect and defect to valence band. A particularly problematic situation for photovoltaic applications would therefore be the situation, where $E_{ph}S_{HR} = E_g/2$. In this case, transitions from either band to a midgap defect would be fast and even low midgap defect densities would suffice for fast recombination and low photovoltaic efficiency.

Figure 11c shows that lower phonon energies would, at a constant and sufficiently small value of S_{HR}, lead to longer lifetimes at a given trap density. Figure 11c assumes the energy difference to be 600 meV. Note here that the condition of a constant value of S_{HR} is an important restriction because phonon energy will have an effect on the Huang–Rhys factor with lower phonon energies generally increasing the Huang–Rhys factor.[115] However, the exact dependence $S_{HR}(E_{ph})$ will be affected by the type of electron–phonon coupling dominating (deformation coupling or polar coupling). In addition, the relation between the

reduced mass m_r of the atomic oscillator and the phonon energy (approximately inverse, i.e., $m_r \sim 1/E_{ph}$)[115] will affect the result. Therefore, we will not provide a detailed discussion of the compensation of the beneficial effect of lower phonon energies as shown in Figure 11c by a potential increase of the Huang–Rhys factor with phonon energy but highlight the necessity of further studies on this topic. Figure 11d shows how the lifetime depends on the Huang–Rhys factor indicating that as long as $S_{HR} < p$, any increase in S_{HR} will lead to shorter lifetimes. Once the minimum at $S_{HR} = p$ is reached, a further increase of S_{HR} will lead to longer lifetimes.

Thus, in order to achieve long lifetimes, we conclude that low defect densities, low Huang–Rhys factors, and low phonon energies should be important ingredients. Future work on understanding the relation between molecular and crystal structures and these parameters is important. For the prominent case of perovskites, low deep defect densities have already been observed and identified[20,124] as a key ingredient for their long lifetimes and high open-circuit voltages. In molecules and molecular semiconductors, the concept of a phonon is no longer strictly applicable. Nevertheless, the general principle of the energy-gap law remains valid.[125–129] For the case of organic photovoltaics, Benduhn et al.[128] have used the high energies of the vibrational modes of the lightweight elements used for organic semiconductors (i.e., ≈160 meV for the C=C bond) as

**ADVANCED
SCIENCE NEWS**

www.advancedsciencenews.com

**ADVANCED
ENERGY
MATERIALS**

www.advenergymat.de

an explanation for the high losses due to nonradiative recombination in these materials. Recently, the field of organic photovoltaics was transformed by the advent of new small molecule but nonfullerene acceptors that enable higher open-circuit voltages (relative to the polymer absorption onsets) as opposed to fullerene-based organic solar cells.[130–147] These open-circuit voltages are enabled by a combination of lower offsets between the lowest occupied molecular orbital of the donor and the acceptor leading to higher charge transfer state energies and by lower nonradiative voltage losses $\Delta V_{oc,nrad}$. In the context of the energy gap law, we understand the latter effect of lower $\Delta V_{oc,nrad}$ as being a result of the increased charge transfer state energy.

In the case of ligand-capped PbS quantum dots, Bozyigit et al.[148] have studied multiphonon processes using thermal admittance spectroscopy and inelastic neutron scattering. One of the key results was the observation that the modification of the surface ligands is likely not affecting the passivating defects, i.e., altering N_t in Equations (38) and (39) but instead the ligands affect the mechanical properties of the surface of nanocrystals and thereby the Huang–Rhys factor and the amount of electron–phonon coupling. Bozyigit et al. also raise a currently unresolved problem, namely, the combination of the equations for multiphonon recombination as derived by Ridley,[115,116] Markvart,[114,120] and others with the concept of the Meyer–Neldel rule[149] that considers the effect of entropy on increasing transitions involving many phonons.

6.3. The Role of the Effective Density of States on Photovoltaic Performance

The effective mass m_{eff} or effective density of states N_{eff} that is directly related via $N_{eff} \propto m_{eff}^{3/2}$ is a great example illustrating the whole chain of going from microscopic properties to estimates of photovoltaic performance using different levels of abstraction. Low values of the effective mass have been cited in the literature as being useful for achieving high mobilities[46] and high open-circuit voltages.[150] While the arguments used in these papers are correct while taken in isolation, the question of whether high or low effective masses are useful for photovoltaic performance is much less obvious if all effects of effective masses are considered in combination. Effective mass or effective densities of state (DOS) affect absorption coefficients (see Equation (36)), recombination rates (via their influence on the equilibrium charge carrier concentrations), and mobilities. The result depends on various properties of the material and the device, i.e., whether the material is a direct or indirect semiconductor, whether the material is doped or not, and in case of mobility which scattering model dominates transport. We discuss all these different scenarios in a separate publication.[151] Here, we will just briefly review the key ideas for one simple scenario assuming a direct, intrinsic semiconductor $(\alpha = \alpha_0 \sqrt{(E - E_g)/kT})$. The effect of effective mass m_{eff} on mobility μ is described typically by the equation $\mu = q\tau_m/m_{eff}$,[112] with τ_m being the momentum relaxation time that depends on effective mass as well. Depending on the scattering model, there are therefore various dependencies between mobility and effective mass possible of which we choose one for illustration purposes, namely $\mu \propto m_{eff}^{-5/2}$ (scattering via

zero-order optical phonons).[112] In addition, we will not distinguish between effective masses of conduction and valence band, and just assume them to be identical for simplicity. The calculation of the efficiency for high mobilities can then be done using Equations (30)–(32) with J_{sc} given by Equation (10) with the quantum efficiency calculated using perfect collection and light trapping (Equation (19)). For finite mobilities, the calculation has to be done using a drift–diffusion simulation software (ASA[109] in this case) solving the equations as discussed in Section 5.1 but without taking photon recycling into account.

Figure 12a shows how the prefactor α_0 of the absorption coefficient, the inverse equilibrium recombination rate τ/n_0, and the mobility as a function of the effective density of states N_{eff}. Higher N_{eff} leads to better absorption, because more states are available, but recombination and mobility become slightly worse. Figure 12b shows how the maximum efficiency (solid lines) as a function of thickness changes with effective DOS when we assume the mobility to be infinitely high and the SRH lifetime $\tau = 100$ ns. The higher absorption for higher N_{eff} leads to J_{sc} (dotted lines) increasing and saturating at a lower thicknesses. The higher the thickness, the lower the V_{oc} (dashed lines) will become. This combination of trends leads to an optimum efficiency that is slightly increasing with lower density of states. However, the thickness required to reach that optimum increases as well.

Figure 12c,d shows the efficiency, J_{sc}, and V_{oc} as a function of thickness for the case where the mobility is finite and given by $\mu = \mu_0(m/m_{eff})^{5/2}$. Within each panel, we varied μ_0 which assumes the values $\mu_0 = 10^{-3}$, 10^{-1}, 10 cm^2 V^{-1} s^{-1} (black, dark gray, and light gray lines). Figure 12c shows the case for a lower effective DOS ($N_{eff} = 10^{18}$ cm^{-3}) and Figure 12d for a higher DOS ($N_{eff} = 10^{20}$ cm^{-3}). As previously observed in Figure 12b, the lower effective DOS requires higher thicknesses to achieve full collection and a high J_{sc} (dotted lines). The higher thicknesses necessary for the low effective DOS are partly compensated by the higher mobilities and reduced recombination rates. The final result is that in this example, the lower effective DOS leads to a slightly higher peak efficiency; however, it also requires thicker layers and is therefore not necessarily the better option for a technological implementation. Thus, we conclude that the effective mass is a typical example of a parameter whose influence on photovoltaic performance is varied and complex with the different effects mostly compensating each other.

7. Summary and Outlook

The primary goal of the present paper was to provide a clear recipe how to connect fundamental material properties with a proper thermodynamic description of a solar cell made from the specific material. Such an approach must be able to be consistent with the SQ approach as the ultimate reference. Depending on the amount of input parameters, there are different variations and extensions of the SQ approach that may be used for relating material properties to device functionality. In the SQ limit itself, only band gap and temperature are used to calculate efficiency. Related to the SQ limit are approaches
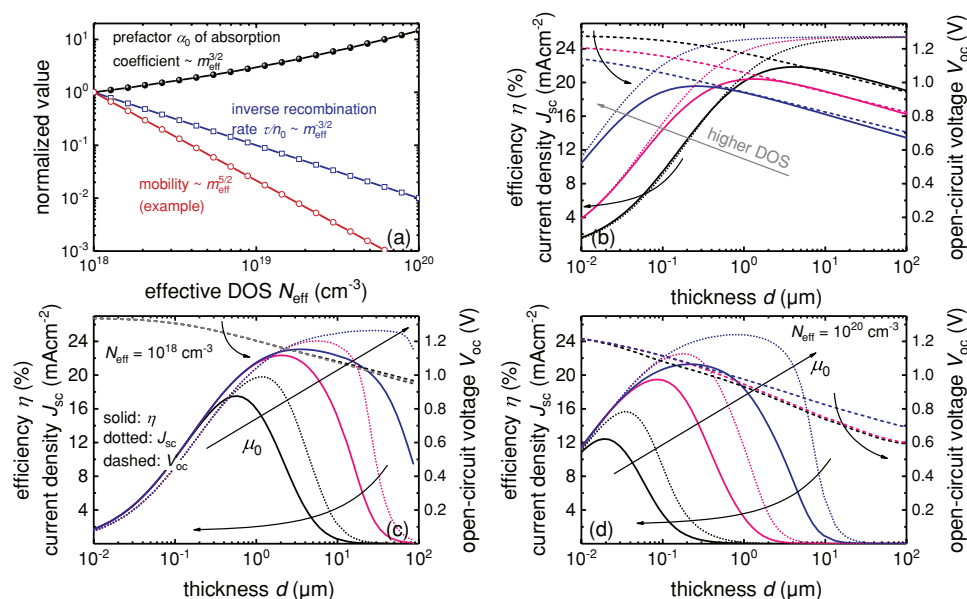
**ADVANCED
SCIENCE NEWS**

www.advancedsciencenews.com

**ADVANCED
ENERGY
MATERIALS**

www.advenergymat.de

Figure 12. a) Dependence of the prefactor α_0 of the absorption coefficient ($\alpha = \alpha_0 \sqrt{(E - E_g)/kT}$), the inverse equilibrium recombination rate τ/n_0, and the mobility as a function of the effective density of states N_{eff} (conduction and valence band DOS assumed equal). b) Efficiency (solid lines), J_{sc} (dotted lines), and V_{oc} (dashed lines) assuming infinite mobilities for three different values of the effective DOS ($N_{eff} = 10^{18}$, 10^{19}, 10^{20} cm^{-3}). Lower DOS leads to slightly higher optimum efficiency but also at higher optimum thicknesses. c,d) Efficiency (solid lines), J_{sc} (dotted lines), and V_{oc} (dashed lines) assuming finite mobilities depending on effective mass as $\mu = \mu_0(m/m_{eff})^{5/2}$ for two different values of the effective DOS ((c) $N_{eff} = 10^{18}$ cm^{-3} and (d) 10^{20} cm^{-3}).

to describe the solar cell based on external, measureable properties such as the external solar cell quantum efficiency and the external luminescence quantum efficiency. However, if one wants to relate true material properties, for instance, obtained by ab initio calculations, one needs to be able to relate, e.g., the "internal" luminescence quantum efficiency (as opposed to the "external" luminescence quantum efficiency) to photovoltaic performance. In this situation, a consistent description requires knowledge of its complex refractive index combined with an optical model which has to make assumptions with regard to the light-trapping scheme. We also show that any assessment of performance based on material properties has to make some assumptions on the absorber layer thickness. We propose here to always scan the whole range of thicknesses and compare efficiencies at the optimum thickness. In order to study the influence of the structure of materials, we have to relate properties such as the effective mass, the phonon energy, or the dielectric permittivity to properties such as absorption coefficient, mobility, and charge carrier lifetime.

While there is no simple general answer to our title question, there are a range of microscopic material properties that have been identified as either beneficial or detrimental for photovoltaic performance and future work is likely to identify more. A key criterion is to have a low likelihood of deep defects that maximize multiphonon transition rates as achieved, for instance, in lead-halide perovskites.[20,124] Another one is to avoid the combination of low band gaps and light elements due to the energy gap law and the occurrence of high-energy vibrational modes in semiconductors made from light elements such as organic semiconductors.[128] A third criterion is

the impact of mechanical properties controlled, for instance, by the choice of ligands in quantum dot solids, where the stiffness of the ligands affects the Huang–Rhys factor and subsequently nonradiative recombination.[148] An example for a relatively influential parameter that cannot directly be regarded as either clearly positive or negative is the effective mass and effective density of states. Both parameters are related and affect absorption coefficient, recombination rates, and mobilities, and therefore have a substantial influence on photovoltaic functionality that is, however, largely cancelling each other out if efficiencies are compared at the optimized thickness.

Future work may use the methods outlined in this progress report and investigate how additional microscopic parameters such as the dielectric permittivity of the material, the polarizability of the material, the phonon energy, the deformation potential constant, the reduced mass of the atomic oscillator, and others affect photovoltaic functionality. It is our hope and aim that a continuation of this work will lead to an improved methodology not only to interpret and explain the performance of actual photovoltaic materials but also to identify promising candidates via computational or experimental material screening studies.

Acknowledgements

**ADVANCED
SCIENCE NEWS**

www.advancedsciencenews.com

**ADVANCED
ENERGY
MATERIALS**

www.advenergymat.de

Conflict of Interest

The authors declare no conflict of interest.

Keywords

[1] N. M. Haegel, R. Margolis, T. Buonassisi, D. Feldman, A. Froitzheim, R. Garabedian, M. Green, S. Glunz, H. M. Henning, B. Holder, I. Kaizuka, B. Kroposki, K. Matsubara, S. Niki, K. Sakurai, R. A. Schindler, W. Tumas, E. R. Weber, G. Wilson, M. Woodhouse, S. Kurtz, *Science* **2017**, *356*, 141.

[2] F. Creutzig, P. Agoston, J. C. Goldschmidt, G. Luderer, G. Nemet, R. C. Pietzcker, *Nat. Energy* **2017**, *2*, 17140.

[3] M. M. Lee, J. Teuscher, T. Miyasaka, T. N. Murakami, H. J. Snaith, *Science* **2012**, *338*, 643.

[4] A. Kojima, K. Teshima, Y. Shirai, T. Miyasaka, *J. Am. Chem. Soc.* **2009**, *131*, 6050.

[5] J. H. Im, C. R. Lee, J. W. Lee, S. W. Park, N. G. Park, *Nanoscale* **2011**, *3*, 4088.

[6] J. H. Heo, S. H. Im, J. H. Noh, T. N. Mandal, C. S. Lim, J. A. Chang, Y. H. Lee, H. j. Kim, A. Sarkar, Md. K. Nazeeruddin, M. Gratzel, S. I. Seok, *Nat. Photonics* **2013**, *7*, 486.

[7] Best Research Cell Efficiencies, https://www.nrel.gov/pv/assets/images/efficiency-chart.png, (accessed: February 2018).

[8] A. M. Ganose, C. N. Savory, D. O. Scanlon, *Chem. Commun.* **2017**, *53*, 20.

[9] C. N. Savory, A. Walsh, D. O. Scanlon, *ACS Energy Lett.* **2016**, *1*, 949.

[10] S. K. Wallace, K. Svane, W. P. Huhn, T. Zhu, D. B. Mitzi, V. Blum, A. Walsh, *Sustainable Energy Fuels* **2017**, *1*, 1339.

[11] X. G. Zhao, J. H. Yang, Y. Fu, D. Yang, Q. Xu, L. Yu, S. H. Wei, L. Zhang, *J. Am. Chem. Soc.* **2017**, *139*, 2630.

[12] Y. Yin, Y. Huang, Y. Wu, G. Chen, W. J. Yin, S. H. Wei, X. Gong, *Chem. Mater.* **2017**, *29*, 9429.

[13] X. G. Zhao, D. Yang, Y. Sun, T. Li, L. Zhang, L. Yu, A. Zunger, *J. Am. Chem. Soc.* **2017**, *139*, 6718.

[14] D. Yang, J. Lv, X. Zhao, Q. Xu, Y. Fu, Y. Zhan, A. Zunger, L. Zhang, *Chem. Mater.* **2017**, *29*, 524.

[15] L. Yu, A. Zunger, *Phys. Rev. Lett.* **2012**, *108*, 068701.

[16] L. P. Yu, S. Lany, R. Kykyneshi, V. Jieratum, R. Ravichandran, B. Pelatt, E. Altschul, H. A. S. Platt, J. F. Wager, D. A. Keszler, A. Zunger, *Adv. Energy Mater.* **2011**, *1*, 748.

[17] S. Chakraborty, W. Xie, N. Mathews, M. Sherburne, R. Ahuja, M. Asta, S. G. Mhaisalkar, *ACS Energy Lett.* **2017**, *2*, 837.

[18] S. Korbel, M. A. L. Marques, S. Botti, *J. Mater. Chem. C* **2016**, *4*, 3157.

[19] J. Hachmann, R. Olivares-Amaya, A. Jinich, A. L. Appleton, M. A. Blood-Forsythe, L. R. Seress, C. Roman-Salgado, K. Trepte, S. Atahan-Evrenk, S. Er, S. Shrestha, R. Mondal, A. Sokolov, Z. Bao, A. Aspuru-Guzik, *Energy Environ. Sci.* **2014**, *7*, 698.

[20] R. E. Brandt, V. Stevanoviç, D. S. Ginley, T. Buonassisi, *MRS Commun.* **2015**, *5*, 265.

[21] J. M. Frost, K. T. Butler, F. Brivio, C. H. Hendon, M. van Schilfgaarde, A. Walsh, *Nano Lett.* **2014**, *14*, 2584.

[22] P. Jackson, D. Hariskos, R. Wuerz, O. Kiowski, A. Bauer, T. M. Friedlmeier, M. Powalla, *Phys. Status Solidi RRL* **2015**, *9*, 28.

[23] P. Jackson, R. Wuerz, D. Hariskos, E. Lotter, W. Witte, M. Powalla, *Phys. Status Solidi RRL* **2016**, *10*, 583.

[24] M. A. Green, K. Emery, Y. Hishikawa, W. Warta, E. D. Dunlop, *Prog. Photovoltaics* **2016**, *24*, 3.

[25] J. L. Shay, S. Wagner, H. M. Kasper, *Appl. Phys. Lett.* **1975**, *27*, 89.

[26] S. Wagner, P. M. Bridenbaugh, *J. Cryst. Growth* **1977**, *39*, 151.

[27] D. Hariskos, P. Jackson, W. Hempel, S. Paetel, S. Spiering, R. Menner, W. Wischmann, M. Powalla, *IEEE J. Photovoltaics* **2016**, *6*, 1321.

[28] T. M. Friedlmeier, P. Jackson, A. Bauer, D. Hariskos, O. Kiowski, R. Wuerz, M. Powalla, *IEEE J. Photovoltaics* **2015**, *5*, 1487.

[29] E. Avancini, R. Carron, B. Bissig, P. Reinhard, R. Menozzi, G. Sozzi, S. Di Napoli, T. Feurer, S. Nishiwaki, S. Buecheler, A. N. Tiwari, *Prog. Photovoltaics* **2017**, *25*, 233.

[30] T. Feurer, P. Reinhard, E. Avancini, B. Bissig, J. Löckinger, P. Fuchs, R. Carron, T. P. Weiss, J. Perrenoud, S. Stutterheim, S. Buecheler, A. N. Tiwari, *Prog. Photovoltaics* **2017**, *25*, 645.

[31] F. Pianezzi, P. Reinhard, A. Chirila, B. Bissig, S. Nishiwaki, S. Buecheler, A. N. Tiwari, *Phys. Chem. Chem. Phys.* **2014**, *16*, 8843.

[32] A. Chirila, P. Reinhard, F. Pianezzi, P. Bloesch, A. R. Uhl, C. Fella, L. Kranz, D. Keller, C. Gretener, H. Hagendorfer, D. Jaeger, R. Erni, S. Nishiwaki, S. Buecheler, A. N. Tiwari, *Nat. Mater.* **2013**, *12*, 1107.

[33] D. Abou-Ras, S. S. Schmidt, N. Schäfer, J. Kavalakkatt, T. Rissom, T. Unold, R. Mainz, A. Weber, T. Kirchartz, E. Simsek Sanli, P. A. van Aken, Q. M. Ramasse, H. J. Kleebe, D. Azulay, I. Balberg, O. Millo, O. Cojocaru-Miredin, D. Barragan-Yani, K. Albe, J. Haarstrich, C. Ronning, *Phys. Status Solidi RRL* **2016**, *10*, 363.

[34] W. Zhang, G. E. Eperon, H. J. Snaith, *Nat. Energy* **2016**, *1*, 16048.

[35] S. D. Stranks, H. J. Snaith, *Nat. Nanotechnol.* **2015**, *10*, 391.

[36] M. A. Green, A. Ho-Baillie, H. J. Snaith, *Nat. Photonics* **2014**, *8*, 506.

[37] J. P. Correa-Baena, M. Saliba, T. Buonassisi, M. Grätzel, A. Abate, W. Tress, A. Hagfeldt, *Science* **2017**, *358*, 739.

[38] S. D. Stranks, G. E. Eperon, G. Grancini, C. Menelaou, M. J. P. Alcocer, T. Leijtens, L. M. Herz, A. Petrozza, H. J. Snaith, *Science* **2013**, *342*, 341.

[39] D. W. deQuilettes, S. Koch, S. Burke, R. K. Paranji, A. J. Shropshire, M. E. Ziffer, D. S. Ginger, *ACS Energy Lett.* **2016**, *1*, 438.

[40] S. De Wolf, J. Holovsky, S. J. Moon, P. Löper, B. Niesen, M. Ledinsky, F. J. Haug, J. H. Yum, C. Ballif, *J. Phys. Chem. Lett.* **2014**, *5*, 1035.

[41] B. Conings, J. Drijkoningen, N. Gauquelin, A. Babayigit, J. D'Haen, L. D'Olieslaeger, A. Ethirajan, J. Verbeeck, J. Manca, E. Mosconi, F. D. Angelis, H. G. Boyen, *Adv. Energy Mater.* **2015**, *5*, 1500477.

[42] T. Leijtens, G. E. Eperon, N. K. Noel, S. N. Habisreutinger, A. Petrozza, H. J. Snaith, *Adv. Energy Mater.* **2015**, *5*, 1500963.

[43] L. Serrano-Lujan, N. Espinosa, T. T. Larsen-Olsen, J. Abad, A. Urbina, F. C. Krebs, *Adv. Energy Mater.* **2015**, *5*, 1501119.

[44] A. Babayigit, D. Duy Thanh, A. Ethirajan, J. Manca, M. Muller, H. G. Boyen, B. Conings, *Sci. Rep.* **2016**, *6*, 18721.

[45] A. Babayigit, A. Ethirajan, M. Muller, B. Conings, *Nat. Mater.* **2016**, *15*, 247.

[46] F. Giustino, H. J. Snaith, *ACS Energy Lett.* **2016**, *1*, 1233.

[47] S. Öz, J. C. Hebig, E. Jung, T. Singh, A. Lepcha, S. Olthof, F. Jan, Y. Gao, R. German, P. H. M. van Loosdrecht, K. Meerholz, T. Kirchartz, S. Mathur, *Sol. Energy Mater. Sol. Cells* **2016**, *158*, 195.

[48] J. C. Hebig, I. Kühn, J. Flohre, T. Kirchartz, *ACS Energy Lett.* **2016**, *1*, 309.

[49] M. H. Kumar, S. Dharani, W. L. Leong, P. P. Boix, R. R. Prabhakar, T. Baikie, C. Shi, H. Ding, R. Ramesh, M. Asta, M. Graetzel, S. G. Mhaisalkar, N. Mathews, *Adv. Mater.* **2014**, *26*, 7122.

[50] P. P. Boix, S. Agarwala, T. M. Koh, N. Mathews, S. G. Mhaisalkar, *J. Phys. Chem. Lett.* **2015**, *6*, 898.

[51] D. Cortecchia, H. A. Dewi, J. Yin, A. Bruno, S. Chen, T. Baikie, P. P. Boix, M. Grätzel, S. Mhaisalkar, C. Soci, N. Mathews, *Inorg. Chem.* **2016**, *55*, 1044.

**ADVANCED
SCIENCE NEWS**

www.advancedsciencenews.com

**ADVANCED
ENERGY
MATERIALS**

www.advenergymat.de

[52] B. Saparov, F. Hong, J. P. Sun, H. S. Duan, W. Meng, S. Cameron, I. G. Hill, Y. Yan, D. B. Mitzi, *Chem. Mater.* **2015**, *27*, 5622.

[53] A. J. Lehner, D. H. Fabini, H. A. Evans, C. A. Hebert, S. R. Smock, J. Hu, H. B. Wang, J. W. Zwanziger, M. L. Chabinyc, R. Seshadri, *Chem. Mater.* **2015**, *27*, 7137.

[54] M. R. Filip, G. E. Eperon, H. J. Snaith, F. Giustino, *Nat. Commun* **2014**, *5*, 5757.

[55] G. Volonakis, M. R. Filip, A. A. Haghighirad, N. Sakai, B. Wenger, H. J. Snaith, F. Giustino, *J. Phys. Chem. Lett.* **2016**, *7*, 1254.

[56] M. Saliba, T. Matsui, J. Y. Seo, K. Domanski, J. P. Correa-Baena, M. K. Nazeeruddin, S. M. Zakeeruddin, W. Tress, A. Abate, A. Hagfeldt, M. Gratzel, *Energy Environ. Sci.* **2016**, *9*, 1989.

[57] D. P. McMeekin, G. Sadoughi, W. Rehman, G. E. Eperon, M. Saliba, M. T. Hörantner, A. Haghighirad, N. Sakai, L. Korte, B. Rech, M. B. Johnston, L. M. Herz, H. J. Snaith, *Science* **2016**, *351*, 151.

[58] M. Saliba, T. Matsui, K. Domanski, J. Y. Seo, A. Ummadisingu, S. M. Zakeeruddin, J. P. Correa-Baena, W. R. Tress, A. Abate, A. Hagfeldt, M. Grätzel, *Science* **2016**, *354*, 206.

[59] A. J. Lehner, H. B. Wang, D. H. Fabini, C. D. Liman, C. A. Hebert, E. E. Perry, M. Wang, G. C. Bazan, M. L. Chabinyc, R. Seshadri, *Appl. Phys. Lett.* **2015**, *107*, 131109.

[60] W. Shockley, H. J. Queisser, *J. Appl. Phys.* **1961**, *32*, 510.

[61] C. H. Henry, *J. Appl. Phys.* **1980**, *51*, 4494.

[62] A. Marti, G. L. Araujo, *Sol. Energy Mater. Sol. Cells* **1996**, *43*, 203.

[63] U. Rau, F. Einsele, G. C. Glaeser, *Appl. Phys. Lett.* **2005**, *87*, 171101.

[64] T. Markvart, *J. Appl. Phys.* **2006**, *99*, 026101.

[65] T. Kirchartz, K. Taretto, U. Rau, *J. Phys. Chem. C* **2009**, *113*, 17958.

[66] L. J. A. Koster, S. E. Shaheen, J. C. Hummelen, *Adv. Energy Mater.* **2012**, *2*, 1246.

[67] J. H. Werner, S. Kolodinski, H. J. Queisser, *Phys. Rev. Lett.* **1994**, *72*, 3851.

[68] M. C. Hanna, A. J. Nozik, *J. Appl. Phys.* **2006**, *100*, 074510.

[69] T. Kirchartz, U. Rau, *Thin Solid Films* **2009**, *517*, 2438.

[70] P. W. Bridgman, *Phys. Rev.* **1928**, *31*, 101.

[71] G. Kirchhoff, *Ann. Phys.* **1860**, *185*, 275.

[72] P. Würfel, *J. Phys. C: Solid State Phys.* **1982**, *15*, 3967.

[73] American Society for Testing and Materials, *Reference Solar Spectral Irradiance: Air Mass 1.5*, NREL, Golden, CO **2017**.

[74] T. Kirchartz, J. Nelson, U. Rau, *Phys. Rev. Appl.* **2016**, *5*, 054003.

[75] U. Rau, *Phys. Rev. B* **2007**, *76*, 085303.

[76] U. Rau, *IEEE J. Photovoltaics* **2012**, *2*, 169.

[77] A. Gerber, V. Huhn, T. M. H. Tran, M. Siegloch, Y. Augarten, B. E. Pieters, U. Rau, *Sol. Energy Mater. Sol. Cells* **2015**, *135*, 35.

[78] K. Yoshikawa, H. Kawasaki, W. Yoshida, T. Irie, K. Konishi, K. Nakano, T. Uto, D. Adachi, M. Kanematsu, H. Uzu, K. Yamamoto, *Nat. Energy* **2017**, *2*, 17032.

[79] D. Bi, W. Tress, M. I. Dar, P. Gao, J. Luo, C. Renevier, K. Schenk, A. Abate, F. Giordano, J. P. Correa Baena, J. D. Decoppet, S. M. Zakeeruddin, M. K. Nazeeruddin, M. Grätzel, A. Hagfeldt, *Sci. Adv.* **2016**, *2*, e1501170.

[80] U. Rau, B. Blank, T. C. M. Müller, T. Kirchartz, *Phys. Rev. Appl.* **2017**, *7*, 044016.

[81] J. Z. Yao, T. Kirchartz, M. S. Vezie, M. A. Faist, W. Gong, Z. C. He, H. B. Wu, J. Troughton, T. Watson, D. Bryant, J. Nelson, *Phys. Rev. Appl.* **2015**, *4*, 014020.

[82] R. T. Ross, *J. Chem. Phys.* **1967**, *46*, 4590.

[83] G. Smestad, H. Ries, *Sol. Energy Mater. Sol. Cells* **1992**, *25*, 51.

[84] M. A. Green, *Prog. Photovoltaics* **2012**, *20*, 472.

[85] T. Kirchartz, A. Helbig, W. Reetz, M. Reuter, J. H. Werner, U. Rau, *Prog. Photovoltaics* **2009**, *17*, 394.

[86] T. Kirchartz, U. Rau, *J. Appl. Phys.* **2007**, *102*, 104510.

[87] T. Kirchartz, U. Rau, M. Kurth, J. Mattheis, J. H. Werner, *Thin Solid Films* **2007**, *515*, 6238.

[88] T. Kirchartz, F. Staub, U. Rau, *ACS Energy Lett.* **2016**, *1*, 731.

[89] B. Blank, T. Kirchartz, S. Lany, U. Rau, *Phys. Rev. Appl.* **2017**, *8*, 024032.

[90] T. Tiedje, E. Yablonovitch, G. D. Cody, B. G. Brooks, *IEEE Trans. Electron Devices* **1984**, *31*, 711.

[91] M. A. Green, *Prog. Photovoltaics* **2002**, *10*, 235.

[92] W. Shockley, W. T. Read, *Phys. Rev.* **1952**, *87*, 835.

[93] R. N. Hall, *Phys. Rev.* **1952**, *87*, 387.

[94] C.-T. Sah, W. Shockley, *Phys. Rev.* **1958**, *109*, 1103.

[95] B. E. Pieters, K. Decock, M. Burgelman, R. Stangl, T. Kirchartz, in *Advanced Characterization Techniques for Thin Film Solar Cells* (Eds: D. Abou-Ras, T. Kirchartz, U. Rau), Wiley-VCH Verlag GmbH & Co. KGaA, Weinheim, Germany **2011**, p. 501.

[96] M. A. Green, *IEEE Trans. Electron Devices* **1984**, *31*, 671.

[97] A. Richter, S. W. Glunz, F. Werner, J. Schmidt, A. Cuevas, *Phys. Rev. B* **2012**, *86*, 165202.

[98] A. Richter, M. Hermle, S. W. Glunz, *IEEE J. Photovoltaics* **2013**, *3*, 1184.

[99] W. van Roosbroeck, W. Shockley, *Phys. Rev.* **1954**, *94*, 1558.

[100] P. Asbeck, *J. Appl. Phys.* **1977**, *48*, 820.

[101] U. Rau, U. W. Paetzold, T. Kirchartz, *Phys. Rev. B* **2014**, *90*, 035211.

[102] R. Brendel, H. J. Queisser, *Sol. Energy Mater. Sol. Cells* **1993**, *29*, 397.

[103] J. Mattheis, J. H. Werner, U. Rau, *Phys. Rev. B* **2008**, *77*, 085203.

[104] J. Mattheis, in *Mobility and Homogeneity Effects on the Power Conversion Efficiency of Solar Cells*, Shaker, Herzogenrath, Germany **2008**, p. 140.

[105] A. Marti, J. L. Balenzategui, R. F. Reyna, *J. Appl. Phys.* **1997**, *82*, 4067.

[106] T. Kirchartz, U. Rau, in *Advanced Characterization Techniques for Thin Film Solar Cells* (Eds: D. Abou-Ras, T. Kirchartz, U. Rau), Wiley-VCH Verlag GmbH & Co. KGaA, Weinheim, Germany **2011**, p. 1.

[107] U. Rau, G. Kron, J. H. Werner, *J. Phys. Chem. B* **2003**, *107*, 13547.

[108] T. Kirchartz, J. Bisquert, I. Mora-Sero, G. Garcia-Belmonte, *Phys. Chem. Chem. Phys.* **2015**, *17*, 4007.

[109] B. E. Pieters, J. Krc, M. Zeman, presented at *Conf. Record of the 2006 IEEE 4th World Conf. on Photovoltaic Energy Conversion*, Waikoloa, Hawaii, May **2006**.

[110] M. A. Green, *Solar Cells* **1982**, *7*, 337.

[111] M. A. Green, *Solid-State Electron.* **1981**, *24*, 788.

[112] B. K. Ridley, *Quantum Processes in Semiconductors*, Oxford University Press, Oxford **2013**.

[113] T. Markvart, in *Recombination in Semiconductors* (Ed: P. T. Landsberg), Cambridge University Press, Cambridge **2003**, p. 474.

[114] T. Markvart, *J. Phys. C: Solid State Phys.* **1981**, *14*, L895.

[115] B. K. Ridley, *Solid-State Electron.* **1978**, *21*, 1319.

[116] B. K. Ridley, *J. Phys. C: Solid State Phys.* **1978**, *11*, 2323.

[117] K. Huang, A. Rhys, *Proc. R. Soc. London, Ser. A* **1950**, *204*, 406.

[118] C. H. Henry, D. V. Lang, *Phys. Rev. B* **1977**, *15*, 989.

[119] S. M. Sze, *Physics of Semiconductor Devices*, John Wiley & Sons, New York, NY **1981**.

[120] T. Markvart, in *Recombination in Semiconductors* (Ed: P. T. Landsberg), Cambridge University Press, Cambridge **2003**, p. 467.

[121] T. Markvart, in *Recombination in Semiconductors* (Ed: P. T. Landsberg), Cambridge University Press, Cambridge **2003**, p. 475.

[122] R. Pässler, *Phys. Status Solidi B* **1976**, *78*, 625.

[123] T. Kirchartz, T. Markvart, U. Rau, D. A. Egger, *J. Phys. Chem. Lett.* **2018**, *9*, 939.

[124] W. J. Yin, T. Shi, Y. Yan, *Appl. Phys. Lett.* **2014**, *104*, 063903.

[125] M. Bixon, J. Jortner, J. Cortes, H. Heitele, M. E. Michel-Beyerle, *J. Phys. Chem.* **1994**, *98*, 7289.

[126] A. Nitzan, S. Mukamel, J. Jortner, *J. Chem. Phys.* **1975**, *63*, 200.

[127] I. R. Gould, D. Noukakis, L. Gomez-Jahn, R. H. Young, J. L. Goodman, S. Farid, *Chem. Phys.* **1993**, *176*, 439.

**ADVANCED
SCIENCE NEWS**
www.advancedsciencenews.com

**ADVANCED
ENERGY
MATERIALS**
www.advenergymat.de

[128] J. Benduhn, K. Tvingstedt, F. Piersimoni, S. Ullbrich, Y. Fan, M. Tropiano, K. A. McGarry, O. Zeika, M. K. Riede, C. J. Douglas, S. Barlow, S. R. Marder, D. Neher, D. Spoltore, K. Vandewal, *Nat. Energy* **2017**, *2*, 17053.

[129] J. S. Wilson, N. Chawdhury, M. R. A. Al-Mandhary, M. Younus, M. S. Khan, P. R. Raithby, A. Köhler, R. H. Friend, *J. Am. Chem. Soc.* **2001**, *123*, 9412.

[130] Y. Lin, F. Zhao, Y. Wu, K. Chen, Y. Xia, G. Li, S. K. K. Prasad, J. Zhu, L. Huo, H. Bin, Z. G. Zhang, X. Guo, M. Zhang, Y. Sun, F. Gao, Z. Wei, W. Ma, C. Wang, J. Hodgkiss, Z. Bo, O. Inganas, Y. Li, X. Zhan, *Adv. Mater.* **2017**, *29*, 1604155.

[131] W. Zhao, S. Li, H. Yao, S. Zhang, Y. Zhang, B. Yang, J. Hou, *J. Am. Chem. Soc.* **2017**, *139*, 7148.

[132] F. Zhao, S. Dai, Y. Wu, Q. Zhang, J. Wang, L. Jiang, Q. Ling, Z. Wei, W. Ma, W. You, C. Wang, X. Zhan, *Adv. Mater.* **2017**, *29*, 1700144.

[133] T. Liu, X. Pan, X. Meng, Y. Liu, D. Wei, W. Ma, L. Huo, X. Sun, T. H. Lee, M. Huang, H. Choi, J. Y. Kim, W. C. H. Choy, Y. Sun, *Adv. Mater.* **2017**, *29*, 1604251.

[134] L. Yang, S. Zhang, C. He, J. Zhang, H. Yao, Y. Yang, Y. Zhang, W. Zhao, J. Hou, *J. Am. Chem. Soc.* **2017**, *139*, 1958.

[135] G. Zhang, G. Yang, H. Yan, J. H. Kim, H. Ade, W. Wu, X. Xu, Y. Duan, Q. Peng, *Adv. Mater.* **2017**, *29*, 1606054.

[136] H. Bin, Y. Yang, Z. G. Zhang, L. Ye, M. Ghasemi, S. Chen, Y. Zhang, C. Zhang, C. Sun, L. Xue, C. Yang, H. Ade, Y. Li, *J. Am. Chem. Soc.* **2017**, *139*, 5085.

[137] P. Cheng, M. Zhang, T. K. Lau, Y. Wu, B. Jia, J. Wang, C. Yan, M. Qin, X. Lu, X. Zhan, *Adv. Mater.* **2017**, *29*, 1605216.

[138] D. Liu, B. Yang, B. Jang, B. Xu, S. Zhang, C. He, H. Y. Woo, J. Hou, *Energy Environ. Sci.* **2017**, *10*, 546.

[139] D. Yang, H. Sasabe, T. Sano, J. Kido, *ACS Energy Lett.* **2017**, *2*, 2021.

[140] G. Zhang, K. Zhang, Q. Yin, X. F. Jiang, Z. Wang, J. Xin, W. Ma, H. Yan, F. Huang, Y. Cao, *J. Am. Chem. Soc.* **2017**, *139*, 2387.

[141] J. Liu, S. Chen, D. Qian, B. Gautam, G. Yang, J. Zhao, J. Bergqvist, F. Zhang, W. Ma, H. Ade, O. Inganäs, K. Gundogdu, F. Gao, H. Yan, *Nat. Energy* **2016**, *1*, 16089.

[142] H. Bin, L. Gao, Z. G. Zhang, Y. Yang, Y. Zhang, C. Zhang, S. Chen, L. Xue, C. Yang, M. Xiao, Y. Li, *Nat. Commun.* **2016**, *7*, 13651.

[143] Z. Li, K. Jiang, G. Yang, J. Y. L. Lai, T. Ma, J. Zhao, W. Ma, H. Yan, *Nat. Commun.* **2016**, *7*, 13094.

[144] D. Baran, R. S. Ashraf, D. A. Hanifi, M. Abdelsamie, N. Gasparini, J. A. Rohr, S. Holliday, A. Wadsworth, S. Lockett, M. Neophytou, C. J. M. Emmott, J. Nelson, C. J. Brabec, A. Amassian, A. Salleo, T. Kirchartz, J. R. Durrant, I. McCulloch, *Nat. Mater.* **2017**, *16*, 363.

[145] S. Holliday, R. S. Ashraf, A. Wadsworth, D. Baran, S. A. Yousaf, C. B. Nielsen, C. H. Tan, S. D. Dimitrov, Z. Shang, N. Gasparini, M. Alamoudi, F. Laquai, C. J. Brabec, A. Salleo, J. R. Durrant, I. McCulloch, *Nat. Commun.* **2016**, *7*, 11585.

[146] D. Baran, T. Kirchartz, S. Wheeler, S. Dimitrov, M. Abdelsamie, J. Gorman, R. S. Ashraf, S. Holliday, A. Wadsworth, N. Gasparini, P. Kaienburg, H. Yan, A. Amassian, C. J. Brabec, J. R. Durrant, I. McCulloch, *Energy Environ. Sci.* **2016**, *9*, 3783.

[147] S. Holliday, R. S. Ashraf, C. B. Nielsen, M. Kirkus, J. A. Röhr, C. H. Tan, E. Collado-Fregoso, A. C. Knall, J. R. Durrant, J. Nelson, I. McCulloch, *J. Am. Chem. Soc.* **2015**, *137*, 898.

[148] D. Bozyigit, N. Yazdani, M. Yarema, O. Yarema, W. M. M. Lin, S. Volk, K. Vuttivorakulchai, M. Luisier, F. Juranyi, V. Wood, *Nature* **2016**, *531*, 618.

[149] A. Yelon, B. Movaghar, R. S. Crandall, *Rep. Prog. Phys.* **2006**, *69*, 1145.

[150] Y. Zhou, G. Long, *J. Phys. Chem. C* **2017**, *121*, 1455.

[151] T. Kirchartz, U. Rau, Influence of the density of states of electrons and holes on the performance of lead-halide perovskites and other photovoltaic absorber materials, Unpublished.